13

Introduction to plasticity and thermal stresses

This chapter will address two important problems often encountered in the design of structure. In section 2.1, constitutive laws for linearly elastic, isotropic and anisotropic materials are presented. Although linearly elastic material behavior is often assumed in preliminary design work, it is often necessary to study the behavior of structures when the material they are made of yields and begins to deform inelastically.

Two issues will be addressed in this chapter. First, when a material is subjected to a complex state of stress, criteria for predicting the onset of yielding will be presented in section 13.1. Next, the behavior of simple structures operating in the plastic range will be discussed in section 13.2.

The second problem to be addressed in this chapter is the behavior of structures under thermal loading, see section 13.3. Two approaches to this problem will be presented: the direct method, see section 13.3.1, and the constraint method, see section 13.3.3. Applications to various structural configurations are presented in section 13.4.

13.1 Yielding under combined loading

The concept of allowable stress discussed in section 2.2, focuses on the highly idealized case of a structural component subjected to a *single stress component*. The yield criterion is then simply expressed in terms of the single stress component as eq. (2.28).

As depicted in fig. 1.3 on page 6, a differential element of material can be subjected to a number of stress components simultaneously. The question is now: what is the proper yield criterion to be used when *multiple stress components are acting simultaneously?* Consider an aircraft propeller connected to a homogeneous, circular shaft. The engine applies a torque that creates a distribution of shear stress throughout the shaft. On the other hand, the propeller creates a thrust that generates a uniform axial stress distribution over the cross-section. If the torque acts alone, the yield criterion is $\tau_{\max} < \tau_y$, where $\tau_{\max}$ is the maximum shear stress acting in the shaft;

if the axial force acts alone, the corresponding criterion is $\sigma_{\max} < \sigma_y$, where $\sigma_{\max}$ is the maximum axial stress acting in the shaft. In the actual structure, both stress components are acting simultaneously, and it is natural to ask: what is the proper criterion to apply?

13.1.1 Introduction to yield criteria

The yield criteria to be presented in this section are applicable to isotropic, homogeneous materials subjected to general three-dimensional states of stress. Since the material is isotropic, the direction of application of the stress is irrelevant. If the material is subjected to a single stress component, it should yield under the same stress level regardless of the direction in which this stress component is applied. In contrast, if the material is anisotropic, the direction of application of stress is now relevant. For instance, consider a composite material consisting of long fibres, all aligned in a single direction and embedded in a matrix material. Intuitively, if a single stress component is applied along the fiber direction, the material response will be dramatically different from that observed when the stress is applied in the direction transverse to the fiber direction.

For isotropic materials, there is no directional dependency of the yield criterion, even when subjected to a combined state of stress. An arbitrary state of stress can be represented by the six stress components defining the stress tensor at that point, for example, see eq. (1.3). Alternatively, the state of stress can be represented by the three principal stresses, σ_{p1}, σ_{p2}, and σ_{p3} and the orientations of the faces on which they act, see section 1.2.2. If the yield criterion must be independent of directional information because of material isotropy, it is clear that *only the values of the principal stress* should appear in its expression. Alternatively, the yield criterion can be expressed in terms of the three stress invariants defined in eq. (1.21).

It is now convenient to represent a state of stress in the geometric space shown in fig. 13.1 where the magnitudes of the principal stresses are plotted as coordinates in a Cartesian system. For instance, point **S** defined by vector $\underline{S}$ represents the state of stress defined by the principal stresses σ_{p1}, σ_{p2}, and σ_{p3}.

An important experimental finding is that *the application of a hydrostatic state of stress has little effect on the yield condition of a material*. The hydrostatic state of stress is the state of stress that a solid experiences when it is immersed in a pressurized liquid. Clearly, the principal stresses associated with the hydrostatic state of stress are $\sigma_{p1} = \sigma_{p2} = \sigma_{p3} = p$, where p is the *hydrostatic pressure*.

If the material is subjected to an arbitrary state of stress, the stress tensor can be decomposed in the following manner

$$\begin{bmatrix} \sigma_{p1} & 0 & 0 \\ 0 & \sigma_{p2} & 0 \\ 0 & 0 & \sigma_{p3} \end{bmatrix} = p \begin{bmatrix} 1\,0\,0 \\ 0\,1\,0 \\ 0\,0\,1 \end{bmatrix} + \begin{bmatrix} \sigma_{p1} - p & 0 & 0 \\ 0 & \sigma_{p2} - p & 0 \\ 0 & 0 & \sigma_{p3} - p \end{bmatrix}, \tag{13.1}$$

where the first term on the right-hand side of the equation represents a state of hydrostatic stress associated with pressure $p = (\sigma_{p1} + \sigma_{p2} + \sigma_{p3})/3$, and the second

term is the *deviatoric stress tensor*. The deviatoric stress tensor is denoted with an over-bar and defined as

$$\begin{bmatrix} \bar{\sigma}_{p1} & 0 & 0 \\ 0 & \bar{\sigma}_{p2} & 0 \\ 0 & 0 & \bar{\sigma}_{p3} \end{bmatrix} = \begin{bmatrix} \sigma_{p1} - p & 0 & 0 \\ 0 & \sigma_{p2} - p & 0 \\ 0 & 0 & \sigma_{p3} - p \end{bmatrix}. \tag{13.2}$$

By construction, the hydrostatic pressure associated with the deviatoric stress tensor vanishes, $(\bar{\sigma}_{p1} + \bar{\sigma}_{p2} + \bar{\sigma}_{p3})/3 = 0$.

In example 1.3 on page 18 it is shown that the direct stress acting on the octahedral face is given by eq. (1.23) as $\sigma_{\rm oc} = (\sigma_{p1} + \sigma_{p2} + \sigma_{p3})/3$; hence, the hydrostatic stress or pressure is also the direct stress acting on the octahedral face.

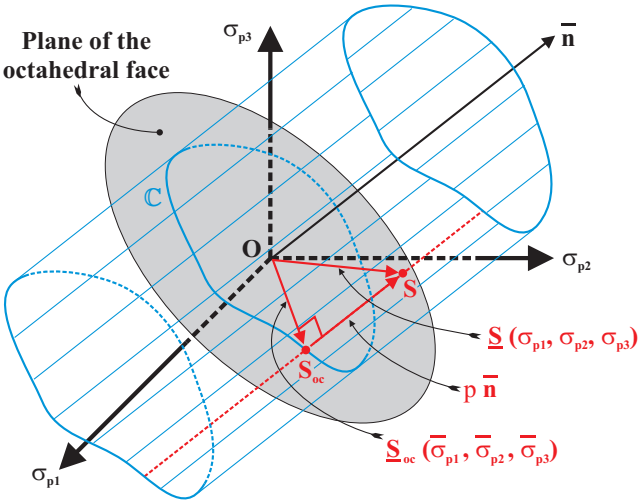

Fig. 13.1. The geometric representation of stress states defined in terms of principal stresses.

In the geometric representation of stress states depicted in fig. 13.1, the plane of the octahedral face is a plane equally inclined with respect to the Cartesian axis system. The equation of this plane is given by $\sigma_{p1} + \sigma_{p2} + \sigma_{p3} = 0$, and unit vector $\bar{n} = \{1, 1, 1\}^T/\sqrt{3}$ is normal to this plane. Let the projection of vector $\underline{S}$ onto the octahedral plane be denoted $\underline{S}_{oc}$. It then follows that the vector equation, $\underline{S} = \underline{S}_{oc} + p\bar{n}$, corresponds to the decomposition of the stress tensor into its hydrostatic and deviatoric parts, as expressed by eq. (13.2). Indeed, vector $\underline{S}_{oc}$ is associated with the stress state $(\sigma_{p1} - p, \sigma_{p2} - p, \sigma_{p3} - p)$.

A important conclusion can now be drawn from this geometric representation. Since the yield condition for the material is unaffected by the addition of a hydrostatic state of stress, the fact that stress state $\underline{S}$ is a yield point implies that $\underline{S}_{oc}$ is also a yield point. In fact, if $\underline{S}$ is a yield point, all the stress points on the line passing through point $\underline{S}$ and parallel to $\bar{n}$ are also yield points. It follows that all yield points

form a cylinder with an axis parallel to $\bar{n}$, and the intersection of this cylinder with the octahedral plane is a curve, denoted $\mathcal{C}$ in fig. 13.1. The locus of the yield points is called the *yield envelope*. This yield envelope is entirely defined by the shape of curve $\mathcal{C}$ that lies in the plane of the octahedral face.

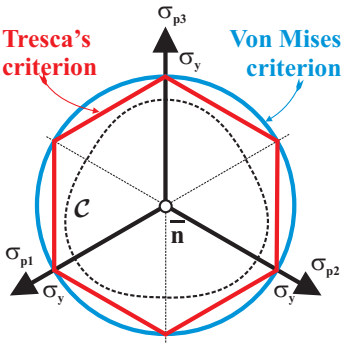

Fig. 13.2. View of the geometric stress space from along unit vector $\bar{n}$; the octahedral face is in the plane of the figure.

The shape of curve $\mathcal{C}$ can be further defined by considering a view of the geometric stress space from along unit vector $\bar{n}$, as depicted in fig. 13.2. In this view, the octahedral face is in the plane of the figure, and the Cartesian axes now appear 120 degrees apart. Because the material is isotropic, if $\underline{S}(\sigma_{p1}, \sigma_{p2}, \sigma_{p3})$ is a yield point, then $\underline{S}'(\sigma_{p2}, \sigma_{p1}, \sigma_{p3})$ is also a yield point. This implies the symmetry of curve $\mathcal{C}$ with respect to axis σ_{p3}. A similar reasoning with the other stress components implies to the symmetry of curve $\mathcal{C}$ with respect to all three axes, σ_{p1}, σ_{p2}, and σ_{p3}. A curve that satisfies these requirement is sketched with a dashed line in fig. 13.2.

In the next two sections, two yield criteria for homogeneous, isotropic materials will be presented. The only difference between the two criteria is the specific shape of curve $\mathcal{C}$, which should be selected to match as closely as possible experimental observation of yield points of such materials under combined stress states.

13.1.2 Tresca's criterion

For Tresca's yield criterion, curve $\mathcal{C}$ is selected to be the regular hexagon shown in fig. 13.2. The complete yield surface is now a regular hexagonal prism with its axis along unit vector $\bar{n}$. In the space of the principal stresses, σ_{p1}, σ_{p2}, and σ_{p3}, the stress states for which the material operates in the linearly elastic range are those stress points falling within this hexagonal prism. This condition can be stated in the following three inequalities derived from the 3 pairs of parallel lines defining the hexagon

$$|\sigma_{p1} - \sigma_{p2}| \leq \sigma_y, \quad |\sigma_{p2} - \sigma_{p3}| \leq \sigma_y, \quad |\sigma_{p3} - \sigma_{p1}| \leq \sigma_y, \tag{13.3}$$

where σ_y is the yield stress observed in a uniaxial test such as described in fig. 2.5. This result is identical to that expressed by eq. (2.29). Applications of Tresca's criterion to simple stress states are discussed in section 2.3.1.

13.1.3 Von Mises' criterion

For von Mises' yield criterion, curve $\mathcal{C}$ is selected to be the circle shown in fig. 13.2. The complete yield surface is now a circular cylinder with its axis along unit vector

$\bar{n}$. In the space of the principal stresses, σ_{p1}, σ_{p2}, and σ_{p3}, the stress states for which the material operates in the linearly elastic range are the stress points falling within this circular cylinder, and therefore the stress states satisfy the following inequality

$$\sigma_{\text{eq}} = \frac{1}{\sqrt{2}}\sqrt{[(\sigma_{p1}-\sigma_{p2})^2+(\sigma_{p2}-\sigma_{p3})^2+(\sigma_{p3}-\sigma_{p1})^2]} \leq \sigma_y, \qquad (13.4)$$

where the first equality defines the *equivalent stress*, σ_{eq}.

Von Mises' criterion now states that *the yield condition is reached under the combined loading, when the equivalent stress, σ_{eq}, reaches the yield stress for a uniaxial stress state, σ_y*. This result is identical to that expressed by eq. (2.32). Applications of Von Mises' criterion to simple stress states are discussed in section 2.3.2.

13.1.4 Problems

Problem 13.1. Alternative formulation of Von Mises' criterion
Consider yield criteria for homogeneous isotropic materials. Justify the following statements: *(1)* material isotropy implies that the yield envelope should be a function only of the invariants of the stress state, and *(2)* the independence of the yield envelope on the addition of a hydrostatic stress state implies that it should be a function only of the invariants of the deviatoric stress tensor. *(3)* Show that the invariant of the deviatoric stress tensor are $\bar{I}_1 = 0$, $\bar{I}_2 = \bar{\sigma}_{p1}\bar{\sigma}_{p2} + \bar{\sigma}_{p2}\bar{\sigma}_{p3} + \bar{\sigma}_{p3}\bar{\sigma}_{p1} = -(\bar{\sigma}^2_{p1} + \bar{\sigma}^2_{p2} + \bar{\sigma}^2_{p3})/2$, and $\bar{I}_3 = \bar{\sigma}_{p1}\bar{\sigma}_{p2}\bar{\sigma}_{p3} = (\bar{\sigma}^3_{p1} + \bar{\sigma}^3_{p2} + \bar{\sigma}^3_{p3})/3$. *(4)* Show that the yield envelope has the form $y(\bar{I}_2,\ \bar{I}_3) = 0$. *(5)* Show that Von Mises' criterion can be recast in that form.

Problem 13.2. Material sample in cylindrical tube
A cylindrical sample of material is put under a multi-axial stress state by confining it in a thin-walled, elastic tube, then applying a pressure, p, to the sample, as depicted in fig. 13.3. The sample is made of a linearly elastic, isotropic material of Young's modulus E_s, Poisson's ratio ν_s and radius R, whereas the tube has a modulus E_t, Poisson's ratio ν_t and thickness t. It is assumed that the friction forces between the sample and the cylinder are negligible. *(1)* Determine the pressure, q, that arises between the sample and the cylinder. *(2)* Determine the hoop stress in the cylinder. *(3)* If the material sample and confining tube are made of the same material, where will the system yield first? Use von Mises' criterion as a yield criterion. Assume $t/R \ll 1$.

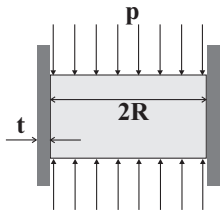

Fig. 13.3. Material sample in cylindrical tube.

13.2 Applications of yield criteria to structural problems

In this section, the yield criteria developed in the previous section will be applied to a number of structural problems. A simple two bar system will be used first to illustrate the basic concepts. Next, the spread of plasticity in a thick tube will be discussed, followed by beam plastic bending and torsion.

Example 13.1. Hyperstatic two-bar system with inelastic behavior

Hyperstatic systems are discussed in section 4.3 and are particularly useful when a structure is expected to be loaded beyond the elastic limit of some of its components. In such cases, the presence of multiple load paths allows the loads to be redistributed among the members that remain elastic, thereby delaying the collapse of the structure.

Consider the two-bar, hyperstatic system depicted in fig. 13.4. Bar **AB** is of length $2L$ and cross-sectional area $\mathcal{A}$, whereas bar **BC** is of length L and cross-sectional area $3\mathcal{A}/2$. Load P is applied at the common point, **B**, of the two bars. Both bars feature the same material with Young's modulus E and yield stress σ_y. The material is assumed to be elastic-perfectly plastic, *i.e.*, the stress-strain diagram is given in fig. 2.7 on page 64.

Intuitively, the system will first operate in the elastic regime with the stress in both bar smaller than σ_y. The solution of this problem is given in example 4.2 on page 141. As the applied load increases, the yield stress will be reached in one of the bar; this load, denoted P^y, is the *elastic limit* of the system. If the load is increased above P^y, one bar operates in the plastic range, *i.e.*, it deforms under constant load, while the other bar still operates in the elastic range. This elastic bar is able to carry additional load because it operates in the elastic regime. If the applied load is increased further, the yield stress is finally reached in the second bar, which now also operates in the plastic range; this load, denoted P^p, is the *plastic limit* of the system. Once this load level is reached, the entire structure now deforms under constant load, and it cannot carry any additional load. Failure occurs when the strain in one of the bar reaches the failure strain, ϵ^f, see fig. 2.7.

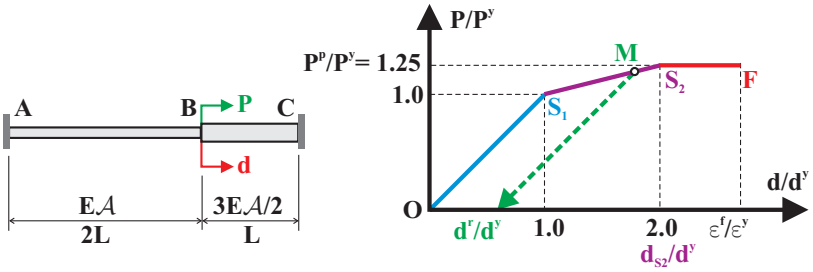

Fig. 13.4. Load-displacement diagram for a two-bar hyperstatic structure with yield stress σ_y.

The displacement method will be used here and follows the steps enumerated in example 4.2. When both bars behave elastically, the equilibrium of the system implies $F_{AB} - F_{BC} = P$, the constitutive laws can be written for each bar as $F_{AB} = e_{AB}\ E\mathcal{A}/(2L)$ and $F_{BC} = e_{BC}\ 3E\mathcal{A}/(2L)$, and finally, the strain-displacement equations imply that $d = e_{AB} = -e_{BC}$, where d is the displacement of point **B**.

The equilibrium equation, written in terms of the unknown displacement, d, becomes $P = [E\mathcal{A}/(2L) + 3E\mathcal{A}/(2L)]d$. This leads to $d = PL/(2E\mathcal{A})$, and the forces in the bars are then

$$F_{AB} = \frac{P}{4}, \quad F_{BC} = -\frac{3P}{4}, \tag{13.5}$$

where the negative sign indicates compression.

Finally, the stresses in the two bar are determined: $\sigma_{AB} = F_{AB}/\mathcal{A} = P/(4\mathcal{A})$ and $\sigma_{BC} = F_{BC}/(3\mathcal{A}/2) = -P/(2\mathcal{A})$. Clearly, bar **BC** is the first to reach the yield level, and hence, the elastic limit of the system is $\sigma_{BC} = -P^y/(2\mathcal{A}) = -\sigma_y$, or $P^y = 2\mathcal{A}\sigma_y$; the corresponding displacement is $d^y = L\sigma_y/E$. Figure 13.4 shows the load-displacement diagram of the system, and portion $\mathbf{OS_1}$ of the curve represents the elastic regime.

If the applied load is increased further, the system enters the elastic-plastic regime: bar **AB** is still elastic, whereas bar **BC** operates in the plastic regime, and $\sigma_{BC} = -\sigma_y$ and $F_{BC} = -3\mathcal{A}\sigma_y/2$. The equilibrium of the system still implies $F_{AB} - F_{BC} = P$, the constitutive laws are $F_{AB} = e_{AB}\, E\mathcal{A}/(2L)$ and $F_{BC} = -3\mathcal{A}\sigma_y/2$, and finally, the strain-displacement equations imply that $d = e_{AB} = -e_{BC}$. The equilibrium equation, written in terms of the unknown displacement becomes $P = 3\mathcal{A}\sigma_y/2 + E\mathcal{A}d/(2L)$, which can be written as

$$\frac{P}{P^y} - 1 = \frac{1}{4}\left(\frac{d}{d^y} - 1\right). \tag{13.6}$$

This is the load-displacement relationship in the elastic-plastic regime represented by portion $\mathbf{S_1S_2}$ of the curve in figure 13.4. The loads in the bar are readily found as

$$\frac{F_{AB}}{P^y} = \frac{P}{P^y} - \frac{3}{4}, \quad \frac{F_{BC}}{P^y} = -\frac{3}{4}. \tag{13.7}$$

If the applied load is increased further, the stress level in bar **AB** now reaches the yield stress, and this happens when the applied load equals P^p, the plastic limit of the structure. At this point, $F_{AB} = \mathcal{A}\sigma_y = P^y/2$, and using eq. (13.7), $1/2 = P^p/P^y - 3/4$, hence

$$\frac{P^p}{P^y} = \frac{5}{4}. \tag{13.8}$$

The corresponding displacement, d^p, is found by introducing the plastic limit into eq. (13.6) to find $d^p/d^y = 2$. The plastic limit point corresponds to point $\mathbf{S_2}$ in fig. 13.4.

If the structure is allowed to operate into the elastic-plastic range up to plastic limit, it can carry a load up to $P^p = 1.25P^y$ which is a 25% increase over the elastic limit load. On the other hand, the apparent stiffness of the structure in the elastic range is $k^y = 2E\mathcal{A}/L$, whereas in the elastic-plastic range, it is reduced to $k^{ep} = E\mathcal{A}/(2L)$, a fourfold decrease.

Above the plastic limit, both bars operate in the plastic regime, the structure deforms continuously under a constant load P^p, and no further increase in applied load is therefore possible. Segment $\mathbf{S_2F}$ of the curve in figure 13.4 represents this fully plastic regime. The structure finally fails when the strain in bar **BC** reaches the compressive failure strain, $-\epsilon^f$, and this happens when the displacement of point **B** equals d^f such that $d^f/d^y = \epsilon^f/\epsilon^y$.

If the structure is loaded into the elastic-plastic range and then unloaded, it behaves elastically because *the stress-strain diagram is linear upon unloading*, see segment **DG** in fig. 2.7. Consider the following scenario: first, the system in loaded to a maximum load, P_m in the elastic-plastic range at point **M** in fig. 13.4, so that $P^y < P_m < P^p$, and then load P_m is released, leaving the structure unloaded. The unloading is equivalent to the application of a reversed load $P_u = -P_m$ at point **M**. Clearly, the system is then unloaded, since the applied load has vanished, $P_m + P_u = 0$. The forces in the bars do not vanish because the initial plastic flow creates permanent deformations.

The remaining forces in the bars after unloading are called *residual forces* and are found by superposing the forces created by the loading in the elastic-plastic range, given in eq. (13.7), with those created by the unloading, given by the negative of eq. (13.5). Note that the elastic solution of eq. (13.5) applies to the unloading because *the material behaves linearly in this regime*. The non-dimensional residual forces in bars **AB** and **BC**, denoted F^r_{AB} and F^r_{BC}, respectively, become

$$\begin{aligned} \frac{F^r_{AB}}{P^y} &= \left(\frac{P_m}{P^y} - \frac{3}{4}\right) - \left(\frac{1}{4}\frac{P_m}{P^y}\right) = \frac{3}{4}\left(\frac{P_m}{P^y} - 1\right), \\ \frac{F^r_{BC}}{P^y} &= \left(-\frac{3}{4}\right) - \left(-\frac{3}{4}\frac{P_m}{P^y}\right) = \frac{3}{4}\left(\frac{P_m}{P^y} - 1\right). \end{aligned} \tag{13.9}$$

The residual forces in bars **AB** and **BC** are tensile and equal. This can be explained as follows. When deformed in the plastic range, bar **BC** undergoes compressive plastic flow. Upon unloading, a permanent residual strain remains in the bar: the bar is now "too short." This is equivalent to a manufacturing imperfection that is created by the permanent plastic deformation of bar **BC**. Imagine that the system is loaded to its plastic limit before unloading, *i.e.*, $P_m = P^p = 1.25P^y$; the resulting residual forces are $F^r_{AB}/P^y = F^r_{BC}/P^y = 3/16$; the residual forces thus represent 18.75% of the elastic limit forces for the system.

It is also interesting to evaluate the residual displacement of point **M** by superposing, once again, the displacements associated with the loading and unloading phases to find

$$\frac{d^r}{d^y} = \left[1 + 4\left(\frac{P_m}{P^y} - 1\right)\right] - \left(\frac{P_m}{P^y}\right) = 3\left(\frac{P_m}{P^y} - 1\right).$$

This is a positive displacement, *i.e.*, in the direction of the applied load P_m, and it is consistent with the permanent shortening of bar **BC** due to plastic deformations. If the system is loaded to its plastic limit before unloading, the residual displacement is $d^r/d^y = 0.75$; the residual displacement therefore represents 75% of the displacement of the structure under the elastic limit load.

Example 13.2. Behavior of a thick-walled tube in the plastic regime

Consider a thick-walled tube with inner and outer radii denoted R_i and R_e, respectively, subjected to an inner pressure p_i. This problem is discussed in example 3.4 on page 122 for a cylinder in plane stress state. Figure 3.8 shows the stress distribution through the thickness of the wall and indicates that the highest stress component is the hoop stress at the inner bore of the cylinder, *i.e.*, at $r = R_i$.

As the inner pressure increases, a critical value is reached for which the material reaches the yield condition at that location. If the pressure is further increased, plasticity will spread in the tube as illustrated in fig. 13.5 where the material is in the plastic regime for $R_i \leq r \leq R_p$ and in the elastic regime for $R_p \leq r \leq R_e$. The radial location, R_p, of the interface between the plastic and elastic regions is an unknown function of the applied pressure.

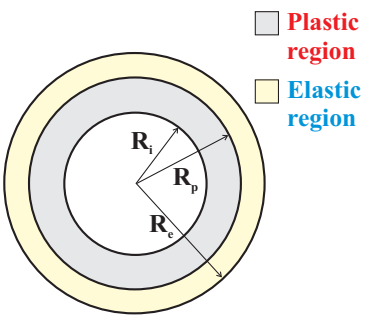

Fig. 13.5. Thick tube under internal pressurization showing the development of concentric plastic and elastic regions.

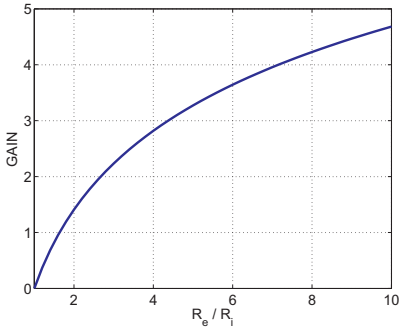

Fig. 13.6. Gain in maximum pressure for a fully plastic tube as compared to the tube operating entirely in the elastic regime.

It will now be assumed that the yield condition is given by Tresca's criterion, see eq. (13.3). Since the stress distribution inside the tube consists of only the radial and hoop stress components without any shear stress, these must be the principal stresses, and hence, $\sigma_{p1} = \sigma_\theta$ and $\sigma_{p2} = \sigma_r$, leading to the following statement for the yield point: $\sigma_\theta - \sigma_r = \sigma_y$, where σ_y is the yield stress for the material.

First, consider the case where the tube is operating entirely in the elastic regime, but it has just reached the yield point for $r = R_i$, *i.e.*, $\sigma_\theta(r = R_i) - \sigma_r(r = R_i) = \sigma_y$. Because the tube is in the elastic regime, the stress field given by eqs. (3.56) is still correct, and introducing these stress components into the yield criterion yields

$$\frac{p_i^y}{\sigma_y} = \frac{1}{2}\left(1 - \frac{R_i^2}{R_e^2}\right). \tag{13.10}$$

This is the maximum internal pressure for which the entire tube remains in the elastic regime.

Next, if pressure is increased further, plasticity spreads into the tube wall. The material is assumed to be elastic-perfectly plastic, *i.e.*, it features the stress-strain diagram illustrated in fig. 2.7 on page 64. The equilibrium condition for the stress components is given by eq. (3.39a), and implies

$$\frac{\mathrm{d}\sigma_r}{\mathrm{d}r} = \frac{\sigma_\theta - \sigma_r}{r} = \frac{\sigma_y}{r}, \tag{13.11}$$

because Tresca's criterion must be exactly satisfied at each point where the elastic-perfectly plastic material is yielding. This equation can be integrated to $\sigma_r/\sigma_y =$

$C_1 + \ln r$, and the boundary condition, $\sigma_r(r = R_i) = -p_i$, is used to evaluate the integration constant, C_1, to find the non-dimensional stress distribution in the plastic zone as

$$\frac{\sigma_r^p}{\sigma_y} = \ln \rho - \frac{p_i}{\sigma_y}, \quad \frac{\sigma_\theta^p}{\sigma_y} = 1 + \ln \rho - \frac{p_i}{\sigma_y}. \tag{13.12}$$

where $\rho = r/R_i$.

Finally, assume that the entire tube operates in the plastic regime, *i.e.*, $R_p = R_e$. An additional boundary condition must then be imposed, $\sigma_r^p(r = R_e) = 0$, to find the corresponding pressure as

$$\frac{p_i^p}{\sigma_y} = \ln \bar{R}_e, \tag{13.13}$$

where $\bar{R}_e = R_e/R_i$.

It is interesting to compare the pressures corresponding to the cylinder operating entirely in the elastic regime, or entirely in the plastic regime, as given by eqs. (13.10) or (13.13), respectively. The increase in load carrying capacity of the tube when it is allowed to operate in the plastic regime is measured by the following index

$$\frac{p_i^p - p_i^y}{p_i^y} = \frac{\ln \bar{R}_e^2}{1 - 1/\bar{R}_e^2}. \tag{13.14}$$

Figure 13.6 shows the gain in maximum pressure as a function of the ratio of external to internal radius; note that for $\bar{R}_e = 2$, the tube can carry an 85% higher internal pressure when operating in the fully plastic range as compared to the elastic range.

The last case to examine is when the tube operates in the mixed elastic-plastic regime. In the elastic zone, the stress field is given by eqs. (3.54)

$$\sigma_r^y = E\left[\frac{C_1}{1-\nu} - \frac{C_2}{(1-\nu)r^2}\right], \; \sigma_\theta^y = E\left[\frac{C_1}{1-\nu} + \frac{C_2}{(1+\nu)r^2}\right],$$

while the stress field in the plastic zone is given by eqs. (13.12).

At the elastic-plastic interface radius $r = R_p$, two conditions must be imposed. First, to satisfy equilibrium, the radial stress components must match across interface: $\sigma_r^p(\rho = \bar{R}_p) = \sigma_r^y(\rho = \bar{R}_p)$, where $\bar{R}_p = R_p/R_i$. Next, from the definition of this interface, the stress fields on either side must satisfy Tresca's yield condition: $\sigma_\theta^P(\rho = \bar{R}_p) - \sigma_\theta^p(\rho = \bar{R}_p) = \sigma_y$ and $\sigma_\theta^y(\rho = \bar{R}_p) - \sigma_\theta^y(\rho = \bar{R}_p) = \sigma_y$, which, in view of the previous condition, implies $\sigma_\theta^p(\rho = \bar{R}_p) = \sigma_\theta^y(\rho = \bar{R}_p)$, Finally, the boundary condition at the outer edge of the cylinder must also be satisfied: $\sigma_r^y(\rho = \bar{R}_e) = 0$. Expressing these three conditions yields the following three equations

$$\begin{aligned}
\ln \bar{R}_p - \frac{p_i}{\sigma_y} &= \frac{EC_1}{(1-\nu)\sigma_y} - \frac{EC_2}{(1+\nu)\sigma_y}\frac{1}{\bar{R}_p^2}, \\
1 + \ln \bar{R}_p - \frac{p_i}{\sigma_y} &= \frac{EC_1}{(1-\nu)\sigma_y} + \frac{EC_2}{(1+\nu)\sigma_y}\frac{1}{\bar{R}_p^2}, \\
\frac{EC_1}{(1-\nu)} &= \frac{EC_2}{(1+\nu)R_e^2},
\end{aligned}$$

which can be solved for the two integration constants, C_1 and C_2, and the unknown interface radius, $\bar{R}_p$. The non-dimensional stress field in the elastic region now becomes

$$\frac{\sigma_r^y}{\sigma_y} = \frac{\bar{R}_p^2}{2}\left(\frac{1}{\bar{R}_e^2} - \frac{1}{\rho^2}\right), \quad \frac{\sigma_\theta^y}{\sigma_y} = \frac{\bar{R}_p^2}{2}\left(\frac{1}{\bar{R}_e^2} + \frac{1}{\rho^2}\right). \tag{13.15}$$

Furthermore, the relationship between the applied pressure and the interface radius, R_p, is

$$\frac{p_i}{\sigma_y} = \frac{1}{2}\left[\ln \bar{R}_p^2 + 1 - \frac{\bar{R}_p^2}{\bar{R}_e^2}\right]. \tag{13.16}$$

In summary, the procedure for computing the response of a thick tube to an increasing internal pressure is as follows. For pressures below the elastic limit given by eq. (13.10), the stress field is that derived in example 3.3, see eq. (3.56). If the applied pressure is above the elastic limit, the tube features both plastic and elastic zones. For a give interface radius, $R_i \leq R_p \leq R_e$, the internal pressure the tube can carry is evaluated with the help of eq. (13.16). The plastic stress field given by eq. (13.12) then applies for $R_i \leq r \leq R_p$, whereas the elastic stress field given by eqs. (13.15) applies for $R_p \leq r \leq R_e$. Finally, the maximum load carrying capability of the tube is the pressure given by eq. (13.13); when that pressure is reached, the tube undergoes continuous plastic flow under constant pressure.

13.2.1 Problems

Problem 13.3. Three bar truss in plastic range
Consider the three bar truss depicted in fig. 4.5. The cross-sectional areas of the homogeneous bars are $\mathcal{A}_A$, $\mathcal{A}_B$, and $\mathcal{A}_C$, for the bars attached at points **A**, **B**, and **C**, respectively, with $\mathcal{A}_A = \mathcal{A}_C$. The three bars are made of an elastic, perfectly plastic material, with material behavior as depicted in fig. 2.7. Let P^y and Δ^y be the maximum load and deflection, respectively, for which the system remains in the linearly elastic range; Let P^p and Δ^p be the load and deflection, respectively, for which the system becomes fully plastic. *(1)* Determine P^y and the corresponding Δ^y. *(2)* Determine P^p and the corresponding elongation on a non-dimensional scale P/P^y vs. Δ/Δ^y. *(4)* Determine the the loading, P^f/P^y, and elongation, Δ^f/Δ^y, of the system at failure. *(5)* Plot the load deformation curve, P/P^y versus Δ/Δ^y, up to failure. *(6)* Assume the load $(P^y + P^p)/2$ is applied to the system, then released. Find the residual stresses in the bar, σ_B^r/σ_y, and σ_C^r/σ_y. Find the residual elongation of the system, Δ^r/Δ^y.

Problem 13.4. Thick-walled cylinder pressurized in the plastic regime
Consider a thick-walled cylinder of internal and external radii R_i and R_e, respectively, in a state of plane stress subjected to an internal pressure p_i. The tube is allowed to operate in the plastic regime; the material is elastic-perfectly plastic and the yield condition is given Tresca's criterion; $R_e/R_i = 2$. *(1)* Plot the non-dimensional interface radius, R_p/R_i, as a function of the non-dimensional pressure, p_i/p_i^E. *(2)* On one graph, plot the radial stress distribution through the thickness of the tube for different values of the interface radius. *(3)* On one graph, plot the hoop stress distribution through the thickness of the tube for different values of the interface radius. For the last two questions, let $R_p = R_i + \alpha(R_e - R_i)$; present your results for $\alpha = 0$, 0.1, 0.2, 0.4, 0.6 and 1.

13.2.2 Plastic bending

The beam theory developed in chapters 5, 6 and 8 assumes that the material a beam is made of behaves in a *linearly elastic* manner following Hooke's law, eq. (5.14). Assuming the beam is made of a ductile material presenting a stress-strain diagram similar to that shown in fig. 2.5 on page 63, once the bending moment applied to the beam generates axial stresses larger than the limit of proportionality, Hooke's law is no longer an appropriate approximation to the constitutive behavior of the material. In this section, beam bending theory is generalized to deal with materials that do not behave in a linearly elastic fashion.

It is important to understand that the Euler-Bernoulli assumptions presented in section 5.1 are *purely kinematic assumptions*. This means that these assumptions imply a specific displacement field for the beam, see eq. (5.4), or equivalently, its strain field, see eq. (5.7). Clearly, these assumptions are independent of the constitutive laws selected to represent the physical behavior of the material.

To simplify the development of the theory, the beam is assumed to present a rectangular section of width b and height h, as depicted in fig. 13.7. The strain distribution is assumed to be linear over the cross-section, as implied by the the Euler-Bernoulli assumptions, see eq. (5.30). The strains at the bottom and top locations of the section are denoted ϵ_b and ϵ_t, respectively, and the corresponding stresses are denoted σ_b and σ_t, respectively. In view of the linear distribution of axial strain, eq. (5.30), it follows that

$$\Delta\epsilon = \epsilon_t - \epsilon_b = -x_{2t}\kappa_3 + x_{2b}\kappa_3 = -(x_{2t} - x_{2b})\kappa_3 = -h\kappa_3. \tag{13.17}$$

where x_{2b} and x_{2t} are the coordinates of the bottom and top locations of the section, respectively.

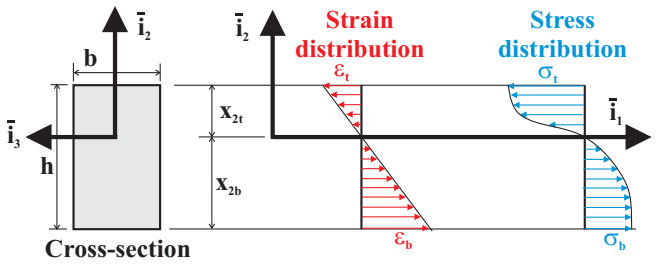

Fig. 13.7. Beam with a rectangular cross-section undergoing plastic bending.

Since the material is not linearly elastic, the stress distribution associated with the assumed linear strain distribution is no longer linear through the cross-section. Figure 13.7 shows the stress distribution through the cross-section. Because the strain is a linear function of vertical position on the cross-section, the vertical stress distribution is, in fact, identical in shape to the stress-strain diagram of the material, rotated by 90 degrees (*i.e.*, the strain axis lies along the vertical axis).

The stress distribution must be in equilibrium with the externally applied loads, and hence, the axial force must vanish, *i.e.*, $N_1 = \int_{\mathcal{A}} \sigma_1 \, \mathrm{d}\mathcal{A} = 0$. Because the section is rectangular, $\mathrm{d}\mathcal{A} = b \, \mathrm{d}x_2$, and furthermore, the linearity of the axial strain distribution, eq. (5.30), implies $\mathrm{d}\epsilon_1 = -\kappa_3 \mathrm{d}x_2$, so that $\mathrm{d}\mathcal{A} = -b/\kappa_3 \, \mathrm{d}\epsilon_1$. The vanishing of the axial force now requires $N_1 = \int_{\mathcal{A}} \sigma_1 \, \mathrm{d}\mathcal{A} = -(b/\kappa_3) \int_{\epsilon_b}^{\epsilon_t} \sigma_1 \, \mathrm{d}\epsilon_1 = 0$. Because the stress is a function of the strain, as implied by the stress-strain diagram for the material, this condition becomes

$$\int_{\epsilon_b}^{\epsilon_t} \sigma_1(\epsilon_1) \, \mathrm{d}\epsilon_1 = 0. \tag{13.18}$$

The physical interpretation of this result is as follows: the area under the stress-strain diagram from ϵ_b to ϵ_t must vanish. If the stress-strain diagram is symmetric for tension and compression, this requirement will be automatically met if $\epsilon_b = -\epsilon_t$, and both strain and stress components will vanish at the geometric center of the section. On the other hand, if the material does not behave in the same manner in tension and compression, the stress-strain diagram is no longer symmetric. Consequently, the strain and stress will then vanish at a point away from the geometric center of the section, and the location of the modulus-weighted centroid defined in eq. 5.33 will now be a function of the applied bending moment.

Next, the bending moment is computed from the axial stress distribution using eq. (5.10) to find

$$M_3 = \int_{\mathcal{A}} \sigma_1 x_2 \, \mathrm{d}\mathcal{A} = \frac{b}{\kappa_3^2} \int_{\epsilon_b}^{\epsilon_t} \sigma_1 \epsilon_1 \, \mathrm{d}\epsilon_1. \tag{13.19}$$

The second integral represents the static moment of the stress-strain diagram computed with respect to the origin. Equation (13.19) gives the relationship between the bending moment and the curvature of the beam in the plastic bending regime.

In practice, the relationship between the bending moment and the curvature is constructed as follows.

1. Select an arbitrary value of the strain ϵ_b. Then, determine the strain ϵ_t such that eq. (13.18) is satisfied. It is now possible to compute the curvature of the beam from $\Delta_\epsilon = \epsilon_t - \epsilon_b = -h\kappa_3$ and hence,

$$\kappa_3 = -\frac{\Delta_\epsilon}{h}. \tag{13.20}$$

2. Determine the location of the centroid. The linearity if the strain distribution implies

$$\frac{|x_{2t}|}{|x_{2b}|} = \frac{|\epsilon_t|}{|\epsilon_b|}. \tag{13.21}$$

3. Compute the bending moment using eq. (13.19).
4. Repeat the above procedure for a number of strain levels, ϵ_b. For each new strain level, a new point of the moment-curvature diagram is obtained. It is then possible to plot $M_3 = M_3(\kappa_3)$; this relationship is nonlinear as a result of the nonlinearity inherent to the stress-strain diagram.

Usually, the stress-strain diagram is obtained empirically, and the above procedure must be carried out numerically for each point defining the diagram. If an analytical expression is available for the stress-strain diagram, the above procedure will yield an analytical expression for the sectional moment-curvature diagram as will be illustrated in the following example.

Example 13.3. Plastic bending for an elastic-perfectly plastic material
In this example, the plastic bending of a rectangular cross-section of width b and height h, made of an elastic-perfectly plastic material is investigated.

The stress-strain diagram for an elastic-perfectly plastic material is given in fig. 2.7 on page 64. In view of the symmetry of this stress-strain diagram, the centroid of the section remains at the geometric center of the rectangular section, as implied by eq. (13.18).

Intuitively, the section will operate in three distinct regimes that are illustrated in fig. 13.8. As the applied bending moment increases, the stress levels will increase until the axial stresses at the top and bottom locations of the section reach the yield stress, σ_y. For stress levels below σ_y, the material behaves in a linearly elastic manner, and the axial stress distribution is linear through the section, see fig. 13.8a. The bending moment that will generate axial stress levels of $|\sigma_y|$ at the top and bottom locations of the section is easily found to be $M_3^y = bh^2\sigma_y/6$, and the corresponding curvature of the beam is evaluated with the help of eq. (13.20) as $\kappa_3^y = -2\epsilon_1^y/h$ where ϵ_1^y is the maximum elastic strain which occurs at the bottom edge of the section.

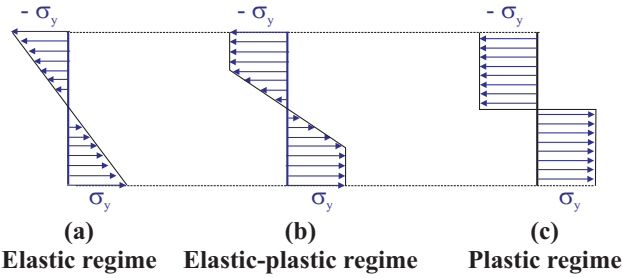

Fig. 13.8. The three regimes of the cross-section: the purely elastic, elastic-plastic, and fully plastic regimes.

If larger bending moments, $M_3 > M_3^y$, are applied, a portion of the section will operate in the plastic regime as shown in fig. 13.8b. In this elastic-perfectly plastic regime, the bending moment is computed with the help of eq. (13.19); for a strain level ϵ_1, the static moment of the stress-strain diagram is

$$\int_{-\epsilon_1}^{\epsilon_1} \sigma_1 \epsilon_1 \, \mathrm{d}\epsilon_1 = \int_{-\epsilon_1}^{-\epsilon_1^y} (-\sigma_y)\, \epsilon_1 \, \mathrm{d}\epsilon_1 + \int_{-\epsilon_1^y}^{\epsilon_1^y} \left(\sigma_y \, \frac{\epsilon_1}{\epsilon_1^y}\right) \epsilon_1 \, \mathrm{d}\epsilon_1 + \int_{\epsilon_1^y}^{\epsilon_1} (\sigma_y)\, \epsilon_1 \, \mathrm{d}\epsilon_1$$
$$= \sigma_y \left(\epsilon_1^2 - \frac{(\epsilon_1^y)^2}{3}\right) = \sigma_y \epsilon_1^2 \left[1 - \frac{1}{3}\left(\frac{\epsilon_1^y}{\epsilon_1}\right)^2\right].$$

The moment-curvature relationship then follows from eq. (13.19) as

$$\begin{aligned} M_3 &= b\sigma_y \frac{\epsilon_1^2}{\kappa_3^2}\left[1 - \frac{1}{3}\left(\frac{\epsilon_1^y}{\epsilon_1}\right)^2\right] = \frac{bh^2}{4}\sigma_y \left[1 - \frac{1}{3}\left(\frac{\kappa_3^y}{\kappa_3}\right)^2\right] \\ &= \frac{3M_3^y}{2}\left[1 - \frac{1}{3}\left(\frac{\kappa_3^y}{\kappa_3}\right)^2\right], \end{aligned} \tag{13.22}$$

where the relationship between strain and curvature, eq. (13.20), is used to eliminate the strains, $h/2 = \epsilon_1^y/\kappa_3^y = \epsilon_1/\kappa_3$.

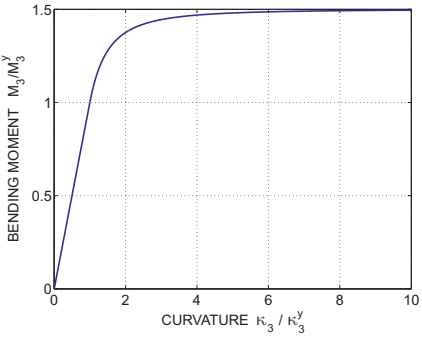

Fig. 13.9. The moment-curvature diagram for a section made of elastic-perfectly plastic material.

As the applied bending moment increases, plasticity spreads in the section until a limit bending moment, M_3^p, is reached for which the associated axial stress distribution is depicted in fig. 13.8c. It is easily verified from this figure that $M_3^p = bh^2/4\ \sigma_y = 3/2\ M_3^y$. At this point, no further increase in applied bending moment can be supported, and any attempt to increase the bending moment will result in an unbounded increase in the curvature. This is illustrated in the complete moment-curvature diagram depicted in fig. 13.9.

In section 2.1.4, it is pointed out that upon unloading, ductile materials tend to behave elastically. For the elastic-perfectly plastic material considered here, if deformed under a stress $|\sigma_1| > \sigma_y$, residual stresses and strains will remain after unloading. The portion of the section for which $|\epsilon_1| > \epsilon_1^y$ will have residual strains after unloading, whereas no residual strains will remain in the portion of the section for which $|\epsilon_1| \leq \epsilon_1^y$. The total strain, which is the sum of the elastic and resid-

ual strains, must remain linearly distributed over the section in accordance with the Euler-Bernoulli kinematics and will not vanish upon unloading.

The unloading can be represented by the application of an unloading moment, M_u, that is equal and opposite to the applied moment, and the residual stresses are evaluated using the following process.

1. First, the beam is loaded into the elastic-plastic range with a moment $M_3^y \leq M_m \leq M_3^p$, and a corresponding curvature, κ_m, develops. The associated axial stress distribution is depicted in fig. 13.10a.
2. Next, an unloading bending moment, denoted $M_u = -M_m$, is applied to the beam. Because the material behaves elastically upon unloading, the stress distribution associated with this unloading moment is the linear distribution depicted in fig. 13.10b.
3. Finally, the residual stresses are obtained by combining these two stress distributions as shown in fig. 13.10c.

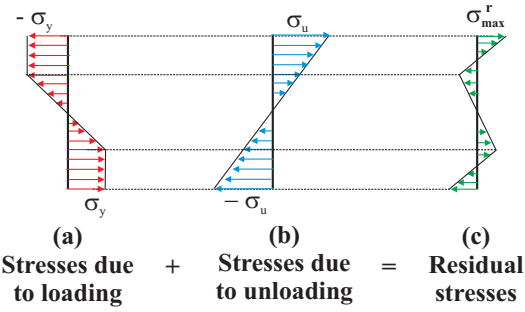

Fig. 13.10. Residual stresses after plastic bending in a section made of elastic-perfectly plastic material.

At the end of this process the beam is unloaded, and the bending moment associated with the residual stress distribution must vanish. From eq. (13.22) the bending moment-curvature relationship is $M_m = 3/2\ (bh^2\sigma_y/6)[1 - (\kappa_3^y/\kappa_m)^2/3]$. The unloading bending moment is related to the maximum unloading axial stress as $M_u = -bh^2/6\ \sigma_u$. Since the total applied load must vanish, $M_u = -M_m$, and the maximum unloading stress becomes

$$\sigma_u = \frac{3\sigma_y}{2}\left[1 - \frac{1}{3}\left(\frac{\kappa_3^y}{\kappa_m}\right)^2\right].$$

The maximum residual stress is found in the outermost point of the section as $\sigma_u - \sigma_y$, see fig. 13.10c; hence

$$\sigma^r_{\max} = \frac{\sigma_y}{2}\left[1 - \left(\frac{\kappa_3^y}{\kappa_m}\right)^2\right] = \sigma_y\left(\frac{M_m}{M_3^y} - 1\right).$$

If the section is unloaded after applying the maximum bending moment $M_m = M_3^p = 3/2\ M_3^y$, the maximum residual stress is $\sigma^r_{\max} = \sigma_y/2$.

13.2.3 Problems

Problem 13.5. Plastic bending of beam with diamond cross-section

Consider a beam with a diamond shaped cross-section of size a by a as shown in fig. 13.11 and made of an elastic-perfectly plastic material. *(1)* Determine the maximum bending moment, M_3^y, for which the section remains in the elastic range and the corresponding curvature κ_3^y. *(2)* Plot the bending moment-curvature diagram for this beam; use non-dimensional abscissa κ_3/κ_3^y and ordinate M_3/M_3^y. *(3)* What is the maximum bending moment, M_3^p/M_3^y, the section can carry when all the material enters the plastic range? *(4)* Find the maximum residual stress in the cross-section if the beam is unloaded after application of a bending moment M_3^p.

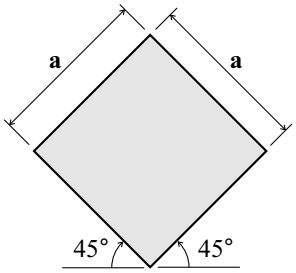

Fig. 13.11. Beam diamond cross-section.

Problem 13.6. Plastic bending of beam with strain hardening

The stress-strain relationship for strain hardening materials can be approximatively represented by Ludwik's power law, $\sigma/C = \epsilon^n$, where C and n are material parameters. Consider a beam with a rectangular cross-section of width b and height h, made of a material that follows Ludwik's power law. *(1)* On one graph, plot the non-dimensional stress, σ/C, versus strain diagrams for n = 0.1, 0.2, 0.3, and 0.5. *(2)* Compute the bending moment versus curvature relationship for the beam. *(3)* On one graph, plot the non-dimensional bending moment, $M_3/(Cbh^2)$, versus non-dimensional curvature, $h\kappa_3$, for n = 0.1, 0.2, 0.3, and 0.5. The material is assumed to have identical behavior in tension and compression, and hence, $\int_{-\epsilon_1}^{\epsilon_1} \sigma_1\epsilon_1\ \mathrm{d}\epsilon_1 = 2\int_0^{\epsilon_1} \sigma_1\epsilon_1\ \mathrm{d}\epsilon_1$.

13.2.4 Plastic torsion

The theory developed for torsion of beams with circular cross-sections in the section 7.1 is based on the assumption that the material behaves in a *linearly elastic* manner, and Hooke's law, eq. (2.9), is assumed to apply. Assuming the circular bar is made of a ductile material presenting a shear stress-shear strain diagram similar to that presented in fig. 2.6 on page 64, once the torque applied to the bar generates shear stresses larger than the limit of proportionality, Hooke's law is no longer an appropriate approximation to the constitutive behavior of the material.

The theory of torsion of cylindrical bars is based on the kinematic description developed in section 7.1.1. Since this kinematic description is obtained from symmetry arguments and does not involve any consideration of constitutive laws, it remains valid for the present case involving materials deformed past their limit of proportionality. The only non-vanishing strain component is the circumferential shear strain,

γ_α, given by eq. (7.9), which is linearly distributed over the circular cross-section as depicted in fig. 7.4. Let γ_M be the maximum circumferential shear strain at the outer edge of the section, and in view of eq. (7.9), $\gamma_M = R\kappa_1$.

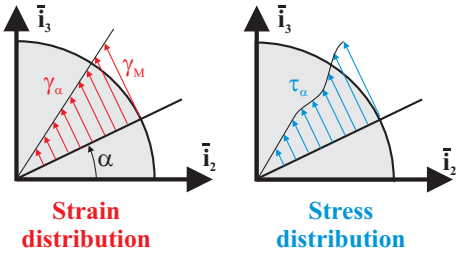

Fig. 13.12. Bar with a circular cross-section undergoing plastic torsion.

Because the material is not linearly elastic, the stress distribution associated with the linear shear strain distribution is no longer the linear stress distribution shown in fig. 7.5. Instead, fig. 13.12 shows the linear shear strain distribution and the associated nonlinear shear stress distribution. This shear stress distribution must be in equilibrium with the externally applied torque

$$\begin{aligned} M_1 &= \int_{\mathcal{A}} \tau_\alpha r \, \mathrm{d}\mathcal{A} = \int_0^{2\pi} \int_0^R \tau_\alpha r \, r \mathrm{d}r \mathrm{d}\theta \\ &= 2\pi \int_0^R \tau_\alpha r^2 \, \mathrm{d}r = \frac{2\pi}{\kappa_1^3} \int_0^{\gamma_M} \tau_\alpha(\gamma_\alpha) \gamma_\alpha^2 \, \mathrm{d}\gamma_\alpha. \end{aligned} \tag{13.23}$$

In this equation, the linear distribution of shear strain, $\gamma_\alpha = r\kappa_1$, is used to eliminate the radial variable r and to express $\mathrm{d}r = \mathrm{d}\gamma_\alpha/\kappa_1$, to facilitate the evaluation of the last integral.

Finally, the shear stress is explicitly a function of the shear strain, $\tau_\alpha = \tau_\alpha(\gamma_\alpha)$, through the material stress-strain diagram. The last integral in eq. (13.23) can be evaluated directly from the stress-strain diagram.

In practice, the relationship between the torque and the twist rate is constructed as follows.

1. Select an arbitrary value of the maximum shear strain γ_M and compute the associated twist rate as $\kappa_1 = \gamma_M/R$.
2. Compute the torque using eq. (13.23) and the material stress-strain diagram.
3. Repeat the above procedure for a number of maximum shear strain levels, γ_M. For each new maximum strain level, a new point of the torque-twist rate diagram is obtained. This relationship will be nonlinear in view of the nonlinearity inherent in the stress-strain diagram.

If an analytical expression is available for the shear stress-shear strain diagram, the above procedure will yield an analytical expression for the sectional torque-twist rate diagram. This situation is illustrated in the example below.

Example 13.4. Plastic torsion for an elastic-perfectly plastic material

Section 13.2.4 describes the general procedure for evaluating the torque-twist rate diagram of a circular bar subjected plastic torsion. This procedure will be applied in this example to a bar made of an elastic-perfectly plastic material presenting the stress-strain diagram given in fig. 2.7 on page 64. The yield shear stress and strain will be denoted τ_y and γ_y, respectively, while γ_f denotes the shear strain at failure.

Intuitively, the section will develop three distinct regimes that are illustrated in fig. 13.13. As the applied torque is increased, the shear stress levels will increase until the stress around the outer edge of the section reaches the yield stress, τ_y. For stress levels below τ_y, the material behaves in a linearly elastic manner, and the shear stress distribution is linear as shown in fig. 13.13a.

The torque that will generate a shear stress level of τ_y around the outer edge of the section is easily found from eq. (7.21) to be

$$M_1^y = \frac{H_{11}\tau_y}{GR} = \pi/2\, R^3\tau_y$$

and the corresponding twist rate for the bar is $\kappa_1^y = \gamma_y/R$.

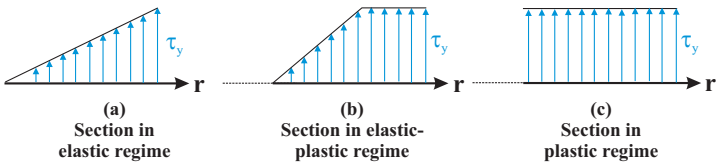

Fig. 13.13. The three stress regimes of the cross-section: (a) purely elastic, (b) elastic-plastic, and (c) fully plastic.

If larger torques, $M_1 > M_1^y$, are applied, a portion of the section will operate in the plastic regime as shown in fig. 13.13b. In this regime, the torque is computed using eq. (13.23). For a shear strain level $\gamma > \gamma_y$, the torque becomes

$$\begin{aligned} M_1 &= \frac{2\pi}{\kappa_1^3}\left[\int_0^{\gamma_y} \tau_y \frac{\gamma}{\gamma_y}\gamma^2\, \mathrm{d}\gamma + \int_{\gamma_y}^{\gamma} \tau_y\gamma^2\, \mathrm{d}\gamma\right] \\ &= \frac{2\pi}{3}\tau_y\left(\frac{\gamma}{\kappa_1}\right)^3\left[1 - \frac{1}{4}\left(\frac{\gamma_y}{\gamma}\right)^3\right] = \frac{4M_1^y}{3}\left[1 - \frac{1}{4}\left(\frac{\kappa_1^y}{\kappa_1}\right)^3\right]. \end{aligned} \tag{13.24}$$

As the twist rate increases, the torque increases more slowly than before, and eventually as $\kappa_1 \to \infty$, it reaches an upper limit, M_1^p. At this point, the entire section operates in the plastic regime as depicted in fig. 13.13c, and the shear stress at all points in the cross section is now at the yield level, τ_y. It is easily verified from this figure that $M_1^p = 2\pi R^3\tau_y/3 = 4/3\, M_1^y$.

A plot of the torque-twist rate relationship (*i.e.*, the force-deformation relationship) is shown in fig. 13.14. Initially, this is a linear relationship because Hooke's

law applies, but for $\kappa_1 > \kappa_1^y$ more and more material of the section reaches the plastic range, and the twist rate increases without bound under a nearly constant torque, M_1^p.

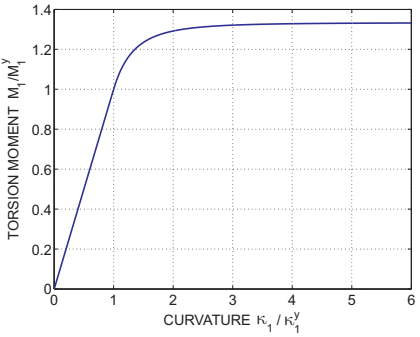

Fig. 13.14. The moment-curvature diagram for a section made of elastic-perfectly plastic material.

Example 13.5. Plastic torsion unloading for an elastic-perfectly plastic material
Consider the unloading of a circular bar twisted beyond its yield stress by the application of a torque $M_1^y \leq M_m \leq M_1^p$. Determine the residual stresses in the section.

In section 2.1.4, it is pointed out that upon unloading, ductile materials tend to behave elastically. For the elastic-perfectly plastic material considered here, if deformed under a stress $|\tau| > \tau_y$, residual stresses and strains will remain after unloading. The portion of the section for which $|\gamma| > \gamma^y$ will present residual strains after unloading, whereas no residual strains will remain in the portion of the section for which $|\gamma| \leq \gamma^y$. The total strain, which is the sum of the elastic and residual strains, must remain linearly distributed over the section in accordance with the kinematic assumptions and will not vanish upon unloading.

The unloading can be represented by the application of an unloading torque, M_u, that is equal and opposite to the applied torque, and the residual stresses are evaluated using the following process.

1. It is first assumed that the bar is loaded into the elastic-plastic range with a torque M_m, and a corresponding twist rate, κ_m, results. The associated shear stress distribution is depicted in fig. 13.13b.
2. Next, an opposing torque (*i.e.*, an unloading torque), denoted $M_u = -M_m$, is applied to the bar. Since the material behaves elastically upon unloading, the shear stress distribution associated with this unloading torque is linear.
3. The residual stresses are obtained by combining these two shear stress distributions. Since at the end of this process the bar is unloaded, the torque associated with the residual stress distribution must vanish.

From eq. (13.24), the relationship between applied torque and curvature is $M_m = 4M_1^y\,[1 - 1/4\,(\kappa_3^y/\kappa_m)^3]/3$. The unloading torque is related to the maximum unloading shear stress as, $M_u = -\pi/2R^3\,\tau_u$, where τ_u is the maximum shear stress at the outer edge of the circular section. Since the net applied torque must vanish, $M_u = -M_m$ and the maximum unloading stress becomes

$$\tau_u = \frac{4\tau_y}{3}\left[1 - \frac{1}{4}\left(\frac{\kappa_3^y}{\kappa_m}\right)^3\right].$$

The maximum residual shear stress is found at the outer edge of the section as $\tau^r_{\max} = \tau_u - \tau_y$,

$$\tau^r_{\max} = \frac{\tau_y}{3}\left[1 - \left(\frac{\kappa_3^y}{\kappa_m}\right)^3\right] = \tau_y\left(\frac{M_m}{M_1^y} - 1\right).$$

If the section is unloaded after applying the maximum torque $M_{max} = M_1^p = 4M_1^y/3$, the maximum residual stress is then $\tau^r_{\max} = \tau_y/3$.

13.3 Thermal stresses in structures

The evaluation of thermal stresses in structures subjected to thermal loading is an important part of structural analysis. Structures such as heat exchangers, jet engine turbine blades, supersonic aircraft and missiles, or space structures must all be designed to withstand significant thermal loading. The thermal loading can have a multitude of effects on structures ranging from induced thermal strain to accelerated viscoelasticity and plasticity.

Simple concepts about thermal stresses are introduced in section 2.1.2, and examples are presented for simple bars as well as isostatic and hyperstatic trusses. This chapter focuses on the computation of thermal stresses in structures arising from thermally induced strains using the theory of linear elasticity. Such problems are generally referred to as *thermoelastic problems.*

Thermal stresses are induced by three main sources: *(1)* nonuniform temperature distributions that create nonuniform strains within a structure, *(2)* external constraints that prevent the free deformation of a structure, and *(3)* differences in coefficients of thermal expansion that appear in heterogeneous structures.

In most practical applications, thermoelastic problems can be treated as *quasi-static, uncoupled problems*. The term "quasi-static" refers to the fact that the temperature variations are slow, and hence, inertia effects associated with the acceleration of the structure under time-dependent temperature fields can be neglected. Thermal stresses are evaluated for different steady temperature distributions, which represent the thermal loading at different instants in time. The term "uncoupled" refers to the fact that generation of heat in the structure is not taken into account. If a structure is subjected to repeated loading, heat is generated through hysteresis, resulting in a nonuniform increase in temperature. Here again, these changes in temperature are slow. The time constants of the resulting heat conduction problem are far slower

than the time constants associated with the dynamic response of the structure, and decoupling the two problems has little effect on the accuracy of the solution.

In a free, unconstrained structure, any thermal stresses must form a system of *self-equilibrating stresses*; indeed, a free body diagram of any portion of the structure reveals that all stress resultants must vanish. If the structure is constrained so that its thermal deformation is prevented by boundary conditions, the thermal stresses will be in equilibrium with the reaction forces at those boundaries.

Two main approaches to the evaluation of thermal stresses are possible. First, the *direct method*, discussed in section 13.3.1, treats thermal problems as basic elasticity problems. While this approach is always possible, it can be cumbersome to apply when dealing with structural components such as beams and plates. In section 13.3.3, the *constraint method* is presented. This method is often much easier to apply to beam and plate problems.

13.3.1 The direct method

When a sample of material is heated, its dimensions will change. Under heat, homogeneous isotropic materials will expand equally in all directions, generating *thermal strains*, $\epsilon^t = f(\Delta T)$, where $f(\Delta T)$ is a function of the change in temperature ΔT. The volume of most materials increases when the material is subjected to increased temperatures, whereas temperature decreases generally cause the material volume to shrink. There are, however, notable exceptions: the transition from water to ice under decreasing temperature is accompanied by a volume increase. For moderate temperature changes, it is often adequate to assume that $f(\Delta T)$ is a linear function of the temperature change so that $f(\Delta T) = \alpha \Delta T$, where α is the *coefficient of thermal expansion*, a positive number if the material expands under increased temperature. The thermal strain now becomes

$$\epsilon^t = \alpha \Delta T. \tag{13.25}$$

Coefficients of thermal expansion for commonly used structural materials are listed in table 13.1.

Table 13.1. Coefficients of thermal expansion and Young's moduli for commonly used structural materials.

Material	Coefficient of thermal expansion [μ/C]	Young's modulus [GPa]
Aluminum	23	73
Copper	17	120
Steel	11	210
Titanium	8.6	110

Two important aspects of thermal deformations must be emphasized. First, thermal strains are purely extensional: temperature changes induce no shear strains. Second, thermal strains do not generate any internal stresses, in contrast with mechanical

strains that are related to internal stresses through the material constitutive law. Consequently, an unconfined material sample subjected to a uniform temperature change simply expands, but no internal stresses are developed.

Thermal strains are the consequence of temperature changes, whereas mechanical strains result from the application of stresses. Hence, it is simpler to state the constitutive law with thermal effects by superposing these strains. The total strains are the sum of the mechanical strains given by eq. (2.4) and their thermal counterparts given by eq. (13.25)

$$\epsilon_1 = \frac{1}{E}\left[\sigma_1 - \nu(\sigma_2 + \sigma_3)\right] + \alpha\Delta T, \tag{13.26a}$$

$$\epsilon_2 = \frac{1}{E}\left[\sigma_2 - \nu(\sigma_1 + \sigma_3)\right] + \alpha\Delta T, \tag{13.26b}$$

$$\epsilon_3 = \frac{1}{E}\left[\sigma_3 - \nu(\sigma_1 + \sigma_2)\right] + \alpha\Delta T. \tag{13.26c}$$

Because temperature changes induce no shear strains, the constitutive laws for shear strain, given by eq. (2.9), remain unchanged and are repeated here

$$\gamma_{23} = \frac{1}{G}\,\tau_{23}, \quad \gamma_{13} = \frac{1}{G}\,\tau_{13}, \quad \gamma_{12} = \frac{1}{G}\,\tau_{12}. \tag{13.27}$$

When dealing with constrained material samples, temperature changes will indirectly generate stresses in the material. For example, consider a bar constrained at its two ends by rigid walls that prevent any extension of the bar. When subjected to a temperature change, ΔT, the bar will expand in all directions, but the rigid walls prevent expansion of the bar along its axis, $\bar{\imath}_1$. The stress components in the transverse direction, σ_2 and σ_3, must vanish because the bar is free to expand in those directions, whereas the axial strain, ϵ_1, must vanish due to the presence of the rigid walls. Equation (13.26a) then implies

$$\epsilon_1 = \frac{1}{E}\sigma_1 + \alpha\Delta T = 0,$$

and hence, $\sigma_1 = -E\alpha\Delta T$; the temperature change thus induces a compressive stress in the bar. Such stresses are called *thermal stresses*. If the same bar is allowed to expand freely, *i.e.*, if the end walls are removed, axial equilibrium of the bar implies $\sigma_1 = 0$ and eq. (13.26a) then yields $\epsilon_1 = \alpha\Delta T$. In this case, the temperature change induces thermal strains but no thermal stresses.

The equations of the theory of elasticity consist of three groups: equilibrium equations, strain-displacement equations, and constitutive laws. As expected, equilibrium equations are unaffected by the presence thermal strains because equilibrium conditions involve forces, not deformations. Strain-displacement equations also remain unchanged, although the strains are now the sum of the mechanical and thermal strains. Only the constitutive laws are directly affected by the presence of thermal strains, see eqs. (13.26).

In summary, the evaluation of thermal stresses based on the theory of three-dimensional elasticity relies on the following three sets of equations: equilibrium

equations, see eqs. (1.4); strain-displacement, see eqs. (1.63) and (1.71); and finally, the constitutive laws, eqs. (13.26) and (13.27), for linearly elastic, isotropic materials.

The direct method will be illustrated by means of several problems that are solved in the following examples.

Example 13.6. Thick circular tube in plane strain state

Consider a thick tube of internal and external radii denoted as R_i and R_e, respectively, subjected to a radially varying temperature field, as shown in fig. 13.15. The temperature of the inner and outer walls of the tube are denoted T_i and T_e, respectively, and heat flow through the tube is assumed to maintain the temperature differential. At thermal equilibrium, the temperature distribution through the thickness of the tube can be shown to be of the form[1]

$$T(r) - T_e = -\frac{T_e - T_i}{\ln \bar{R}_i} \ln \rho, \tag{13.28}$$

where $\rho = r/R_e$ is the non-dimensional radial variable, and $\bar{R}_i = R_i/R_e$.

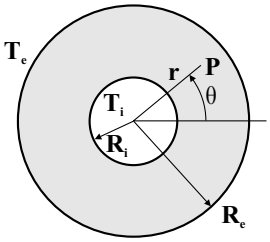

Fig. 13.15. Thick tube in plane strain state subjected to a temperature field.

Both the geometry and thermal loading are axisymmetric and therefore partial derivatives with respect to the circumferential coordinate vanish. The tube is assumed to be in a state of plane strain, *i.e.*, $\epsilon_3 = 0$, which would occur in a long tube constrained at both ends. Imposing the vanishing of the axial strain in eq. (13.26c) then yields $\sigma_3 = \nu(\sigma_r + \sigma_\theta) - E\alpha T$. Introducing this result into eqs. (13.26a) and (13.26b) gives the radial and circumferential stress components as

$$\sigma_r = \frac{E\left[(1-\nu)\epsilon_r + \nu\epsilon_\theta - (1+\nu)\alpha T\right]}{(1-2\nu)(1+\nu)},$$
$$\sigma_\theta = \frac{E\left[\nu\epsilon_r + (1-\nu)\epsilon_\theta - (1+\nu)\alpha T\right]}{(1-2\nu)(1+\nu)}.$$

The strain-displacement equations of the problem are given by eqs. (3.37a) and (3.37b) as $\epsilon_r = \mathrm{d}u_r/\mathrm{d}r$ and $\epsilon_\theta = u_r/r$. The single radial equilibrium equation is $\mathrm{d}\sigma_r/\mathrm{d}r + (\sigma_r - \sigma_\theta)/r = 0$, see eq. (3.39a).

[1] The radial temperature distribution is determined by solution to a heat flow problem that is beyond the scope of this text.

Introducing the above expressions for the stress components into the equilibrium equation and expressing the strains in terms of the radial component of displacement yields the governing equation of the problem as

$$\frac{\mathrm{d}^2 u_r}{\mathrm{d}r^2} + \frac{1}{r}\frac{\mathrm{d}u_r}{\mathrm{d}r} + \frac{u_r}{r^2} - \frac{1+\nu}{1-\nu}\alpha\frac{\mathrm{d}T}{\mathrm{d}r} = 0,$$

which can be put into more compact form as

$$\frac{\mathrm{d}}{\mathrm{d}r}\left[\frac{1}{r}\frac{\mathrm{d}}{\mathrm{d}r}(r u_r)\right] = \frac{1+\nu}{1-\nu}\alpha\frac{\mathrm{d}T}{\mathrm{d}r}.$$

Integrating this equation twice gives the radial displacement distribution as

$$u_r = C_1\, r + \frac{C_2}{r} + \frac{1+\nu}{1-\nu}\frac{\alpha}{r}\int_{R_i}^{r} r\, T\, \mathrm{d}r,$$

where C_1 and C_2 are integration constants.

Because the boundary conditions are expressed in terms of stress components at the inner and outer surfaces, the above solution must now be expressed in terms of stresses. The strains are readily found using the strain-displacement equations, and using the constitutive laws, the stress components become

$$\sigma_r = \frac{E}{1+\nu}\left(\frac{C_1}{1-2\nu} - \frac{C_2}{r^2}\right) - \frac{\alpha E}{1-\nu}\frac{1}{r^2}\int_{R_i}^{r} rT\,\mathrm{d}r,$$
$$\sigma_\theta = \frac{E}{1+\nu}\left(\frac{C_1}{1-2\nu} + \frac{C_2}{r^2}\right) + \frac{\alpha E}{1-\nu}\frac{1}{r^2}\int_{R_i}^{r} rT\,\mathrm{d}r - \frac{E\alpha T}{1-\nu}.$$

The two integration constants are determined from the two boundary conditions: $\sigma_r = 0$ at $r = R_i$ and R_e, as

$$\frac{C_1}{1-2\nu} = \frac{C_2}{R_i^2} = \frac{\alpha}{1-\bar{R}_i^2}\frac{1+\nu}{1-\nu}A,$$

where $A = \int_{\bar{R}_i}^{1} \rho T(\rho)\mathrm{d}\rho$.

The thermal stresses in the thick tube now become

$$\sigma_r = \frac{\alpha E}{1-\nu}\left[\frac{A}{1-\bar{R}_i^2}\left(1 - \frac{\bar{R}_i^2}{\rho^2}\right) - \frac{B(\rho)}{\rho^2}\right],$$
$$\sigma_\theta = \frac{\alpha E}{1-\nu}\left[\frac{A}{1-\bar{R}_i^2}\left(1 + \frac{\bar{R}_i^2}{\rho^2}\right) + \frac{B(\rho)}{\rho^2} - T\right],$$

where $B(\rho) = \int_{\bar{R}_i}^{\rho} \rho T(\rho)\mathrm{d}\rho$.

The axial displacement field is then readily found by substituting C_1 and C_2 into the above expression for u_r as

$$u_r = \alpha R_e \frac{1+\nu}{1-\nu}\left[\frac{A}{1-\bar{R}_i^2}\left(1 - 2\nu + \frac{\bar{R}_i^2}{\rho^2}\right) + \frac{B(\rho)}{\rho^2}\right].$$

To complete the solution process, the integrals A and $B(\rho)$ must be evaluated for the temperature distribution given by eq. (13.28) to find

$$\frac{A}{1-\bar{R}_i^2} = \frac{T_e - T_i}{2\ln \bar{R}_i^2}\left[1 + \frac{\bar{R}_i^2 \ln \bar{R}_i^2}{1-\bar{R}_i^2}\right],$$
$$\frac{B(\rho)}{\rho^2} = \frac{T_e - T_i}{2\ln \bar{R}_i^2}\left[1 - \ln \rho^2 - \frac{\bar{R}_i^2(1-\ln \bar{R}_i^2)}{\rho^2}\right].$$

The results of this analysis are shown in fig. 13.16 for $T_e - T_i < 0$, meaning that the interior surface is hotter than the exterior surface. This occurs when the tube contains a hot fluid. Note the large compressive hoop stress at the inner radius of the cylinder. Since this is a plane strain problem, the axial stress, σ_3, is compressive, except near the outer radius of the cylinder where it is relieved by Poisson's effects.

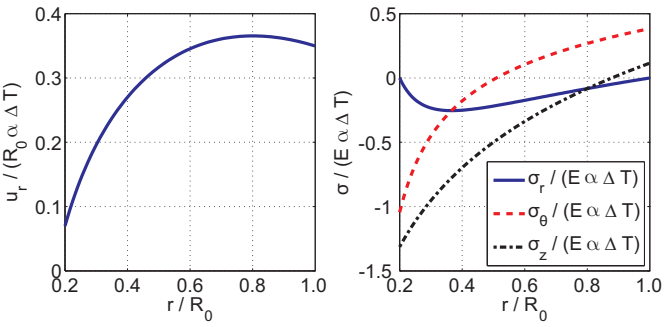

Fig. 13.16. Thermal stresses in a thick tube. Left figure: non-dimensional axial displacement field. Right figure: non-dimensional stress components. $\Delta T = T_e - T_i < 0$.

13.3.2 Problems

Problem 13.7. Thick circular tube in plane stress state

Example 13.6 focused on the determination of the thermal stress field in a thick cylinder in a state of plane strain subjected to the temperature map give by eq. (13.28). Repeat the development presented in example 13.6 for a thick cylinder in a state of plane stress. *(1)* find the radial displacement field. *(2)* Find the radial and hoop stress fields. *(3)* Plot the non-dimensional displacement and stress fields in the format of fig. 13.16.

13.3.3 The constraint method

The constraint method will be developed for a body made of a homogeneous, isotropic material. If the body is free to deform, the thermal strain at any point of the body will be $\epsilon_1^t = \epsilon_2^t = \epsilon_3^t = \alpha T$.

In the first step of the method, the structure is assumed to be *fully constrained*, so that *the thermal deformations are not allowed to take place*. This implies that a set of mechanical strains must appear that exactly compensate for the above thermal strains: $\epsilon_1^m = \epsilon_2^m = \epsilon_3^m = -\alpha T$.

In contrast with the thermal strains that generate no stresses, these mechanical strains are associated with a state of stress given by Hooke's law, eqs. (2.4), such that

$$\sigma_1 = \sigma_2 = \sigma_3 = -\frac{E\alpha T}{1-2\nu}. \tag{13.29}$$

This is a hydrostatic stress state, and introducing these stresses into eq. (2.4a), the first mechanical strain component is found as $\epsilon_1^m = [\sigma_1 - \nu(\sigma_2 + \sigma_3)]/E = -\alpha T$, as expected. Thus, if all thermal deformations are inhibited, the hydrostatic state of stress given by eq. (13.29) must develop at all points of the structure.

To maintain this hydrostatic state of stress in the structure, a set of surface tractions must be applied at the external surface, $\mathcal{S}$, of the body, and body forces must be applied at each point in its volume, $\mathcal{V}$. The constrained surface tractions, $\underline{t}^c$, are readily found from the stress state as

$$\underline{t}^c = -\frac{E\alpha T}{1-2\nu}\bar{n}, \tag{13.30}$$

where $\bar{n}$ is the outer normal to $\mathcal{S}$.

The body forces are easily found by considering the equilibrium equation at a point of the body, eq. (1.4a). Because the shear stresses vanish, this equation reduces to $\partial\sigma_1/\partial x_1 + b_1 = 0$, and the body force component becomes $b_1 = \partial\left[(E\alpha T)/(1-2\nu)\right]/\partial x_1$. Eqs. (1.4b) and (1.4c) yield the other two body force components, and combining these, the constrained body force vector becomes

$$\underline{b}^c = \frac{E\alpha}{1-2\nu}\,\nabla T, \tag{13.31}$$

where ∇ is the gradient operator, $\nabla = \bar{\imath}_1\partial/\partial x_1 + \bar{\imath}_2\partial/\partial x_2 + \bar{\imath}_3\partial/\partial x_3$.

The second step of the procedure calls for the solution of an elasticity problem where the structure is subjected, not to the thermal load but instead, to the set of surface tractions and body forces *opposite* to those required to inhibit thermal deformations. Thus, the structure must be subjected to the following equivalent body forces and surface tractions

$$\underline{b}^e = -\frac{E\alpha}{1-2\nu}\,\nabla\, T, \tag{13.32a}$$

$$\underline{t}^e = \frac{E\alpha T}{1-2\nu}\bar{n}, \tag{13.32b}$$

respectively. In the sequel, these body forces and surface tractions will be called the *equivalent thermal body forces* and *equivalent thermal surface tractions* and denoted with a superscript $(\cdot)^e$.

In third step of the procedure, the solution of the thermal stress problem is found by superposition of the results found in the previous steps. The displacements are

identical to those of the structure subjected to the equivalent thermal loading defined in eq. (13.32), and the thermal stresses are the sum of those generated by the equivalent thermal loading and the constrained hydrostatic stresses given by eq. (13.29).

In summary, the constraint method consists of the following steps.

1. Assume that all thermal deformations are inhibited by a suitable set of body forces and surface tractions given by eqs. (13.31) and (13.30), respectively.
2. Solve an elasticity problem where the structure is subjected to the equivalent thermal body forces and surface tractions given by eqs. (13.32). In this step, the structure is not subjected to thermal effects.
3. Superpose the states of the structures in steps 1 and 2. The displacement of the structure are those found in step 2. The thermal stresses are the sum of those found in step 2 plus the hydrostatic state of stress given by eq. (13.29).

The advantages of the constraint method should be clear. Step 1 is easy, and step 2 is a standard elasticity problem for which all solution procedures developed for elasticity problems can be applied. In fact, the constraint method reduces the evaluation of thermal stresses to a standard isothermal elasticity problem. The equivalent thermal loading given by eqs. (13.32) provides a more intuitive understanding of the response of the structure to a temperature field. Because the constraint method reduces the evaluation of thermal stresses to a standard elasticity problem, it is not very different from the direct method presented in section 13.3.1. Its real advantage becomes evident when applied to bar, beam and plate problems, as discussed in the sections below.

13.4 Application to bars, trusses and beams

The constraint method will be used to solve a number of examples involving axially loaded bars, simple planar trusses, and beams in the following sections and a comparison will be made to the direct method, when appropriate.

13.4.1 Applications to bars and trusses

In section 4.2, the analysis of homogeneous bars with constant properties along their span and subjected to end loads is developed. It is shown that after deformation, the cross-sections remain plane and normal to the axis of the bar. The axial strain also remains uniform over the cross-section. Finally, since the bar is homogeneous, the axial stress is uniformly distributed over the cross-section, and all other stress components vanish.

For such simple structures, the constraint method develop in section 13.3.3 becomes particularly simple. It will be assumed here that each bar is heated to a uniform temperature, T. In step 1 of the approach, thermal deformations are assumed to be inhibited by a suitable set of body forces and surface tractions. Because the stress components σ_2 and σ_2 vanish, Hooke's law implies that the constraint stresses, eq. (13.29), reduce to $\sigma_1 = -E\alpha T$, and $\sigma_2 = \sigma_2 = 0$. In view of eq. (13.31), the

constraint body forces, $\underline{b}^c$, vanish because the temperature field in the bar is uniform, and hence, $\nabla T = 0$. Finally, from eq. (13.30), the constraint surface tractions become forces applied to the bar's ends, $P^c = -E\mathcal{A}\alpha T$, where $\mathcal{A}$ is the cross-sectional area of the bar.

In step 2 of the approach, a bar problem is solved with the thermal equivalent loading consisting of only the thermal equivalent forces, $P^e = E\mathcal{A}\alpha T$, applied to the bar's ends. For trusses constructed from identical members, equivalent forces of magnitude $P^e = E\mathcal{A}\alpha T$ are applied at the ends of each bar. If additional mechanical loads are applied, they are included as well, and the solution proceeds using the procedures developed in previous chapters.

In step 3 of the approach, the solution of the thermal problem is obtained by superposition. The displacements of the bar or truss are those obtained in step 2, and the thermal forces in the bars are obtained superposing the forces obtained in step 2 and the constraint forces, P^c.

Example 13.7. Bar subjected to a uniform temperature

Consider a uniform bar clamped at one end and free at the other, as depicted in the left part of fig. 13.17. The bar is uniformly heated to a temperature T. Find the thermally induced stresses and the deformation in the bar.

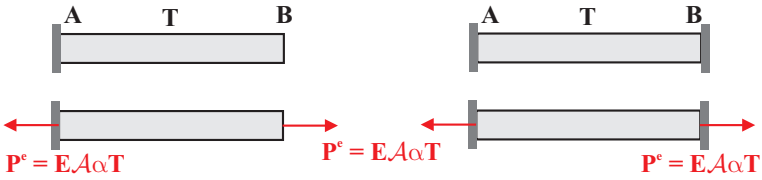

Fig. 13.17. Bar subjected to a uniform temperature. Left figure, the bar is clamped at one end. Right figure, the bar is clamped at both ends.

The constraint method will be used to solve this very simple problem. In step 1 of the approach, the thermal deformations are inhibited by an axial force, $P^c = -E\mathcal{A}\alpha T$. In step 2, equivalent thermal end forces, $P^e = E\mathcal{A}\alpha T$, are applied at points **A** and **B**. The force applied at point **A** is equal to the reaction force at this point. The equivalent problem is a clamped bar subjected to a tip force P^e, and the solution is trivial. The elongation of the bar is given by eq. (4.2) as $e = P^e L/(E\mathcal{A}) = \alpha T L$, and the load in the bar is simply P^e. Finally, in step 3, the deformation of the bar is that found in step 2 for which the displacement at point **B** is $d_B = e = \alpha T L$. The equivalent thermal forces are the superposition of the forces found in steps 1 and 2, $P = P^c + P^e = 0$. As expected, the thermal loads vanish because the bar is free to expand.

If the bar is clamped at both ends, as depicted in the right part of fig. 13.17, the first step of the procedure remains unchanged. In the second step, the equivalent thermal forces P^e are applied at points **A** and **B**, but because these are fixed the bar undergoes no deformation and no stress, and P^e appears as reactions. Finally, in

the last step, the solution of the thermal problem is obtained by superposition of the results from steps 1 and 2. No displacements develop in the system and the thermal loads are the end reactions, $P = P^c + 0 = -E\mathcal{A}\alpha T$. As expected, the thermal forces are compressive.

Example 13.8. Three-bar truss subjected to temperature changes
Consider the three-bar truss depicted in fig. 13.18; the center bar is raised to a temperature T_B, and the two side bars are each raised to a temperature T_A. The side bars have identical Young's modulus E_A, sectional area, $\mathcal{A}_A$, and coefficient of thermal expansion, α_A. The corresponding quantities for the middle bar are E_B, $\mathcal{A}_B$, and α_A, respectively. Find the thermal forces in the system.

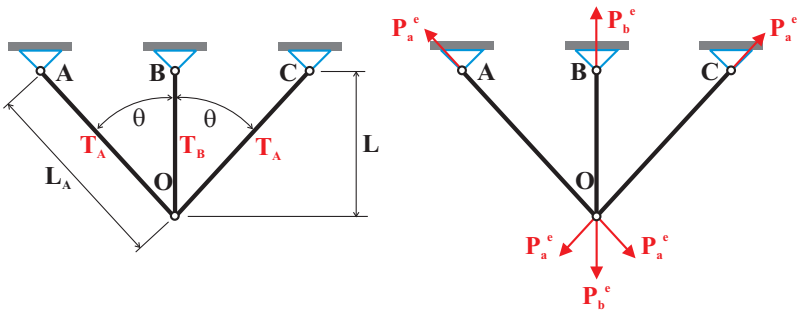

Fig. 13.18. Three-bar truss subjected to temperature changes.

The three-step constraint method is used here again. In the first step, all thermal deformations are inhibited, giving rise to constraint forces in the three bars of $P_A^c = P_C^c = -(E\mathcal{A})_A(\alpha T)_A$ and $P_B^c = -(E\mathcal{A})_B(\alpha T)_B$, respectively.

In the second step, end loads are applied to each bar, and as shown on the right half of fig. 13.18, equivalent thermal end forces $P_A^e = P_C^e = (E\mathcal{A})_A(\alpha T)_A$ and $P_B^e = (E\mathcal{A})_B(\alpha T)_B$ are applied to the side and middle bars, respectively. Clearly, the equivalent thermal forces at the upper ends of the bars are the reaction forces carried at the supports. At point **O**, the total equivalent thermal force is the vector sum of the forces in the three bar, with a net vertical resultant $P_O^e = P_B^e + 2P_A^e \cos\theta$, applied downwards. Step two of the procedure consists of finding the displacements and internal forces in a three-bar truss subjected to the load P_O^e at point **O**. This problem is treated in example 4.4 on page 147, and the vertical deflection, Δ, of point **O** is given by eq. (4.12) as

$$\frac{\Delta}{L} = \frac{(\alpha T)_B + 2\bar{k}_A(\alpha T)_A \cos\theta}{1 + 2\bar{k}_A \cos^3\theta}.$$

while the forces in the bars are given by eq. (4.14) as

$$\frac{F_A^e}{(E\mathcal{A})_B} = \frac{\bar{k}_A \cos^2\theta \left[(\alpha T)_B + 2\bar{k}_A (\alpha T)_A \cos\theta\right]}{1 + 2\bar{k}_A \cos^3\theta},$$
$$\frac{F_B^e}{(E\mathcal{A})_B} = \frac{(\alpha T)_B + 2\bar{k}_A (\alpha T)_A \cos\theta}{1 + 2\bar{k}_A \cos^3\theta}.$$

In step 3 the solution of the thermal problem is found by superposition. The displacement of point **O** is given by the expression above, and the thermal forces are $F_A^t = P_A^c + F_A^e$ and $F_B^t = P_B^c + F_B^e$ for the side and middle bars, respectively,

$$\frac{F_A^t}{(E\mathcal{A})_B} = \frac{\bar{k}_A \left[(\alpha T)_B cos^2\theta - (\alpha T)_A\right]}{1 + 2\bar{k}_A \cos^3\theta},$$
$$\frac{F_B^t}{(E\mathcal{A})_B} = \frac{-2\bar{k}_A \cos\theta \left[(\alpha T)_B cos^2\theta - (\alpha T)_A\right]}{1 + 2\bar{k}_A \cos^3\theta}.$$

As expected, these forces form a set of self-equilibrating forces; it is easily verified that $F_B^t + 2F_A^t \cos\theta = 0$.

First, note that even if the entire structure is heated to a uniform temperature, *i.e.*, if $T_A = T_B$, non-vanishing forces will develop in all three bars. This is a direct consequence of the hyperstatic nature of this problem. If one bar is removed, the problem becomes isostatic and thermal forces will vanish under uniform temperature changes. Second, a three-bar truss problem under simpler thermal loading is treated in example 4.9. Checking that the results obtained in this example reduce to those obtained earlier in example 4.9 on page 159 is left to the reader.

Example 13.9. Deflection of planar truss under thermal loading
The unit load method is developed in section 9.6.6 to evaluate the deflections of truss joints. Equation (9.64) gives the deflection, Δ, at one node of the truss,

$$\Delta = \sum_{i=1}^{N_b} \hat{F}_i \, e_i, \tag{13.33}$$

where $\hat{F}_i$ a set of statically admissible bar forces in equilibrium with a unit load applied at the joint where Δ is to be determined and acting in the direction of Δ. The bar extensions, e_i, are those due to the externally applied loads. Section 9.6.6 presents many examples of application of the unit load method when trusses are subjected to externally applied loads. If thermal deformations are created by changing the temperature of one or more bars in the truss, the unit load method can still be used to determine deflections, but the bar elongations must reflect the induced thermal strains.

If a bar of length L is subjected to end loads, F, and a uniform temperature change, ΔT, its elongation is $e = FL/(E\mathcal{A}) + \alpha \Delta T L$, where the first term is due to the applied load, and the second to the thermal strains. In the presence of thermal deformation, eq. (13.33) now becomes

$$\Delta = \sum_{i=1}^{N_b} \hat{F}_i \, e_i = \sum_{i=1}^{N_b} \hat{F}_i \left(\frac{F_i L_i}{E_i \mathcal{A}_i} + L_i \alpha_i \Delta T_i \right). \tag{13.34}$$

Consider the five-bar, isostatic planar truss subjected to a single external load applied at joint **B**, as depicted in fig. 13.19. All bar have the same physical properties, EA. The tabular format developed in section 9.6.6 is here again. The second column of table 13.2 list the bars flexibility factors and the third the statically admissible forces that are in equilibrium with a unit load acting downward at joint **E**. Column 4 gives the bar forces resulting from the application of the externally applied load, P. Column 5 lists the thermal elongations in each bar, and the last column gives the partial results for the application of eq. (13.34).

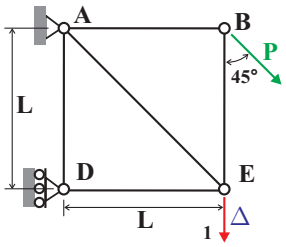

Fig. 13.19. Planar 1-bay truss with thermal loading.

Table 13.2. Calculation of member forces for truss with thermal loading.

Bar	$L_i/(E\mathcal{A})_i$	$\hat{F}_i$	F_i	$L_i\alpha_i\Delta T_i$	$\hat{F}_i[L_i/(E\mathcal{A})_i + L_i\alpha_i\Delta T_i]$
AB	1	0	$P/\sqrt{2}$	1	0
BE	1	0	$-P/\sqrt{2}$	1	0
DE	1	-1	$-P/\sqrt{2}$	1	$-1[-PL/(\sqrt{2}E\mathcal{A}) + L\alpha\Delta T]$
AD	1	0	0	1	0
AE	$\sqrt{2}$	$\sqrt{2}$	P	$\sqrt{2}$	$\sqrt{2}[PL/(E\mathcal{A}) + \sqrt{2}L\alpha\Delta T]$

The vertical deflection of joint **E** is obtained by summing up the entries in the last column of table 13.2 to find

$$\Delta = \frac{3}{\sqrt{2}}\frac{PL}{S} + L\alpha\Delta T.$$

The total deflection is the sum of the joint deflection due to the applied load P (the first term) and of that due to the change in temperature, ΔT, of all bars of the truss (the second term). The thermal deformations of bars **DE** and **AE** are the only contributors to the vertical deflection at joint **E** and are of opposite sign. If the temperature changes for bars **DE** and **AE** are ΔT_{DE} and ΔT_{AE}, respectively, the deflection at joint **E** becomes

$$\Delta = \frac{3}{\sqrt{2}}\frac{PL}{S} + L\alpha(2\Delta T_{AE} - \Delta T_{DE}).$$

It is possible to eliminate the thermal deflection at joint **E** by selecting $2\Delta T_{AE} = \Delta T_{DE}$.

Because this truss is isostatic, bar forces can be evaluated from the equilibrium equations alone; temperature changes do not affect bar forces, only the joint deflections.

13.4.2 Problems

Problem 13.8. Steel bar inside a copper tube
A steel bar with a 750 mm^2 section is placed inside a copper tube with a section of 1250 mm^2. The bar and tube have a common length of 0.5 m and are connected at their ends. At the reference temperature, both elements are stress free. *(1)* If the assembly is heated up of 80° C, find the thermal stresses in both elements using the constraint method. Use the data listed in table 13.1.

Problem 13.9. Rigid plate supported by four elastic bars under thermal loading
Consider the hyperstatic system depicted in fig. 13.20 and consisting of a rigid square plate of side ℓ supported by four identical elastic bars of height h, cross-sectional area $\mathcal{A}$, Young's modulus E, and coefficient of thermal expansion α. The four bars are raised to temperatures T_A, T_B, T_C, and T_D, respectively. Find the thermal forces in the bars using the constraint method. Hint: first study example 4.5.

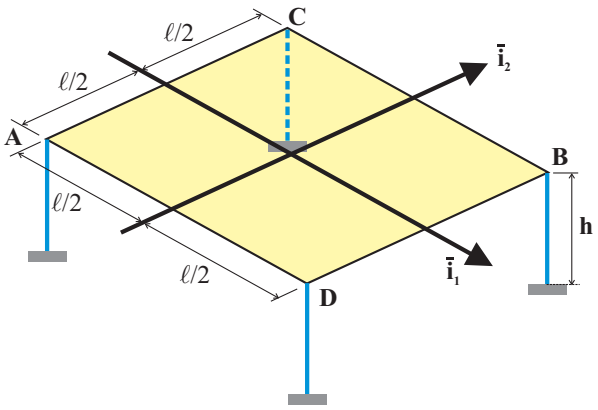

Fig. 13.20. A rigid plate supported by four identical elastic bars.

13.4.3 Application to beams

The constraint method developed in section 13.3.3 will now be applied to beam problems. Rather than starting from the basic equations of elasticity, the Euler-Bernoulli assumptions presented in section 5.1 will form the basis for this development. To simplify the problem, it will be assumed that plane $(\bar{\imath}_1, \bar{\imath}_2)$ is a plane of symmetry for the beam configuration and of the temperature distribution. This implies that the

deformation of the beam will take place in this plane of symmetry. The theory presented in this section could be easily generalized to a beam presenting a cross-section of arbitrary shape and subjected to an arbitrary temperature field. Such developments would be based on the three-dimensional beam theory presented in chapter 6.

As discussed in section 5.4.2, the stresses, σ_2 and σ_3, acting in the plane of the cross-section should remain much smaller than the axial stress component, σ_1. In fact, these stress components can be assumed to vanish, $\sigma_2 \approx 0$ and $\sigma_3 \approx 0$. This leads to the reduced Hooke's law given by eq. (5.14), $\sigma_1 = E\,\epsilon_1$.

In step 1 of the constraint method, thermal deformations are assumed to be fully inhibited. This requires the presence of the following stress system

$$\sigma_1 = -E\alpha T, \quad \sigma_2 = \sigma_3 = 0, \tag{13.35}$$

instead of the hydrostatic state of stress given by eq. (13.29).

Beam theory deals with the stress resultants presented in section 5.3, rather than local stresses. The stress resultants that will fully inhibit thermal deformations consist of an axial force and a bending moment given by eqs. (5.8) and (5.10) as

$$N_1^c = -\int_{\mathcal{A}} E\alpha T \,\mathrm{d}\mathcal{A}, \quad \text{and} \quad M_3^c = \int_{\mathcal{A}} x_2 E\alpha T \,\mathrm{d}\mathcal{A}, \tag{13.36}$$

respectively. Of course, near the end sections of the beam, the actual distribution of axial stress will not be exactly equivalent to this axial force and bending moment. According to Saint-Venant's principle, (principle 2 on page 169), this mismatch is expected to affect only a small portion of the beam, near its end sections.

To equilibrate this distribution of axial forces and bending moments, a set of support loads and bending moments at the boundaries together with distributed axial and transverse loads must be applied to the beam. The end axial loads are simply $P_1^c = N_1^c$ and the end bending moments are $Q_3^c = M_3^c$.

The required distributed axial and transverse loads are found from equilibrium conditions. The axial equilibrium equation for the beam, eq. (5.18), is $p_1 = -\mathrm{d}N_1/\mathrm{d}x_1$, and this implies that the distributed axial load, p_1^c, that equilibrates the constraint axial force is

$$p_1^c = -\frac{\mathrm{d}N_1^c}{\mathrm{d}x_1} = \frac{\mathrm{d}}{\mathrm{d}x_1}\left[\int_{\mathcal{A}} E\alpha T \,\mathrm{d}\mathcal{A}\right]. \tag{13.37}$$

Similarly, the bending equilibrium equation for the beam, eq. (5.39), is $p_2 = \mathrm{d}^2 M_3/\mathrm{d}x_1^2$, leading to the following distribution of transverse loads

$$p_2^c = \frac{\mathrm{d}^2 M_3^c}{\mathrm{d}x_1^2} = \frac{\mathrm{d}^2}{\mathrm{d}x_1^2}\left[\int_{\mathcal{A}} x_2 E\alpha T \,\mathrm{d}\mathcal{A}\right]. \tag{13.38}$$

Step 2 of the constraint method calls for the solution of a beam problem subjected to a set of equivalent end forces and distributed loads opposite to those required to inhibit thermal deformations. Consequently, the beam must then be subjected to the following equivalent thermal end axial forces

$$P_1^e = \int_{\mathcal{A}} E\alpha T \, \mathrm{d}\mathcal{A}. \tag{13.39}$$

and bending moments

$$Q_3^e = -\int_{\mathcal{A}} x_2 E\alpha T \, \mathrm{d}\mathcal{A}. \tag{13.40}$$

Furthermore, the following equivalent thermal distributed axial load

$$p_1^e = -\frac{\mathrm{d}}{\mathrm{d}x_1}\left[\int_{\mathcal{A}} E\alpha T \, \mathrm{d}\mathcal{A}\right], \tag{13.41}$$

and transverse load

$$p_2^e = -\frac{\mathrm{d}^2}{\mathrm{d}x_1^2}\left[\int_{\mathcal{A}} x_2 E\alpha T \, \mathrm{d}\mathcal{A}\right]. \tag{13.42}$$

must also be applied to the beam.

In step 3, the solution of the thermal problem is found by superposition. The displacements of the beam are those found by solving the problem subjected to the equivalent thermal loads. The thermal stresses then are the sum of those found for the same loading, and the stresses required to inhibit thermal deformations. The constraint procedure will be illustrated in the following examples.

Example 13.10. Relationship between the direct and constraint methods

Show that the governing equations for a beam under thermal loading obtained from the constraint method in section 13.4.3 are identical to those obtained by the direct method applied to the classical Euler-Bernoulli beam theory developed in sections 5.4 and 5.5 for beams under axial and transverse loads, respectively.

If the direct method is applied to Euler-Bernoulli beam theory, the kinematic assumptions underpinning the theory remain unchanged, see section 5.1. The equilibrium conditions also remain unchanged, see sections 5.4.3 and 5.5.3 for beams under axial and transverse loads, respectively. The constitutive laws, however, must now reflect the thermal deformation of the beam.

The constitutive laws for beams under axial and transverse loads are discussed in sections 5.4.2 and 5.5.2, respectively. With the addition of thermal effects, eq. (5.14) becomes

$$\sigma_1(x_1, x_2, x_3) = E\,\epsilon_1(x_1, x_2, x_3) - E\alpha\Delta T(x_1, x_2, x_3).$$

Note that in Euler-Bernoulli beam theory, the transverse stress components, σ_2 and σ_3, are assumed to remain much smaller than the axial stress component: $\sigma_2 \ll \sigma_1$ and $\sigma_3 \ll \sigma_1$. In fact, these stress components are assumed to be vanishingly small, leading the reduced version of Hooke's law used here.

In this example, plane $(\bar{\imath}_1, \bar{\imath}_2)$ is assumed to be a plane of symmetry for both the structure and the thermal loading; hence, the deformation of the beam will be entirely contained in this plane. The purely kinematic Euler-Bernoulli assumptions discussed in section 5.1 lead to the same displacement field given by eq. (5.4), which in this case, reduces to $u_1(x_1, x_2, x_3) = \bar{u}_1(x_1) - x_2 \mathrm{d}\bar{u}_2/\mathrm{d}x_1$, $u_2(x_1, x_2, x_3) =$

$\bar{u}_2(x_1)$, and $u_3(x_1, x_2, x_3) = 0$. The corresponding strain field, eq. (5.5), features a single non-vanishing component, the axial strain, which reduces to $\epsilon_1(x_1, x_2, x_3) = \bar{\epsilon}_1(x_1) - x_2\kappa_3(x_1)$. The axial stress now becomes

$$\sigma_1(x_1, x_2, x_3) = E\left[\bar{\epsilon}_1(x_1) - x_2\kappa_3(x_1)\right] - E\alpha\Delta T(x_1, x_2, x_3). \tag{13.43}$$

The axial force in the beam, eq. (5.8), is now readily found as

$$N_1(x_1) = \int_{\mathcal{A}} \left[E\bar{\epsilon}_1 - Ex_2\kappa_3 - E\alpha\Delta T\right] \, \mathrm{d}\mathcal{A} = S\bar{\epsilon}_1(x_1) - P_1^e(x_1), \tag{13.44}$$

where S is the axial stiffness of the beam, eq. (5.17), and P_1^e the equivalent thermal axial force defined by eq. (13.39).

As discussed in section 5.5.2, the origin of the axes system is selected to be at the centroid of the cross-section, implying eq. (5.33). The bending moment in the beam, see eq. (5.10), is found to be

$$M_3(x_1) = -\int_{\mathcal{A}} x_2 \, \left[E\bar{\epsilon}_1 - Ex_2\kappa_3 - E\alpha\Delta T\right] \, \mathrm{d}\mathcal{A} = H_{33}^c\kappa_3(x_1) - Q_3^e(x_1), \tag{13.45}$$

where the bending stiffness of the cross-section, H_{33}^c, is given by eq. (5.36), and the equivalent thermal bending moment, Q_3^e, by eq. (13.40).

To complete the theory, the sectional constitutive laws given above are introduced into the equilibrium equations of the beam to find the governing differential equations of the problem. Introducing the axial force into the axial equilibrium equation, eq. (5.18), leads to

$$\frac{\mathrm{d}}{\mathrm{d}x_1}\left[S\frac{\mathrm{d}\bar{u}_1}{\mathrm{d}x_1}\right] = -\left[p_1(x_1) + p_1^e(x_1)\right], \tag{13.46}$$

where p_1^e is defined by eq. (13.41). When comparing the above equation with eq. (5.19), it is clear that thermal effects introduce an "equivalent thermal axial load," p_1^e, that is simply added to the externally applied axial load, p_1.

Similarly, introducing the bending moment into the transverse equilibrium equation, eq. (5.39), leads to

$$\frac{\mathrm{d}^2}{\mathrm{d}x_1^2}\left[H_{33}^c\frac{\mathrm{d}^2\bar{u}_2}{\mathrm{d}x_1^2}\right] = \left[p_2(x_1) + p_2^e(x_1)\right], \tag{13.47}$$

where p_2^e is defined by eq. (13.42). When comparing the above equation with eq. (5.40), it is clear that thermal effects introduce an equivalent thermal transverse load, p_2^e, that is simply added to the externally applied transverse load, p_2.

Finally, the boundary conditions of the problem must be investigated. Consider a cantilevered beam subjected to a tip axial force, P_1, and a tip bending moment, Q_3. The boundary conditions at the root of the beam are purely kinematic conditions, $\bar{u}_1 = 0$ and $\bar{u}_2 = \mathrm{d}\bar{u}_2/\mathrm{d}x_1 = 0$, that remain unaffected by thermal effects. On the other hand, the natural boundary conditions at the beam's tip are $N_1 = P_1$,

$V_2 = 0$, and $M_3 = Q_3$, that also remain unaffected by thermal effects. When these tip boundary conditions are expressed in terms of the sectional deformation using the sectional constitutive laws, they become $N_1 = S\bar{\epsilon}_1 - P_1^e = P_1$, and $M_3 = H_{33}^c \kappa_3 - Q_3^e = Q_3$. Expressing the sectional deformations in terms of the displacement field then yields the tip boundary conditions as

$$S\frac{\mathrm{d}\bar{u}_1}{\mathrm{d}x_1} = [P_1 + P_1^e], \quad \text{and} \quad H_{33}^c \frac{\mathrm{d}^2\bar{u}_2}{\mathrm{d}x_1^2} = [Q_3 + Q_3^e]. \tag{13.48}$$

Here again, it is clear that thermal effects introduce equivalent thermal axial loads and bending moments, P_1^e and Q_3^e, respectively, that are simply added to the externally applied tip axial force and bending moment.

In conclusion, when the direct method is applied in within the framework of the Euler-Bernoulli assumptions, the governing equations are found to be identical to those of the classical Euler-Bernoulli beam theory, except for the fact that a set of equivalent loads are added to the externally applied loads: the equivalent distributed axial load in eq. (13.46), the equivalent distributed transverse load in eq. (13.47), and the axial force and bending moment at the tip of the beam, see eqs. (13.48). Once this classical beam problem is solved, the axial stresses in the beam are recovered using eq. (13.43). Clearly, this approach is fully consistent with that developed based on the constraint method in section 13.4.3.

Example 13.11. Cantilevered beam under thermal gradient

Consider the cantilevered beam subjected to a parabolic distribution of temperature through the depth, h, of its rectangular cross-section, as shown in fig. 13.21. The temperature of the lower surface of the beam is the reference temperature, $T = 0$, and the temperature of the top surface is $T = T_0$; the temperature profile is $T(x_2) = (x_2/h + 1/2)^2 T_0$.

The equivalent thermal loading shown in fig. 13.21 consists of the end axial load given by eq. (13.39),

$$\begin{aligned} P_1^e &= \int_{\mathcal{A}} E\alpha T \,\mathrm{d}\mathcal{A} = \int_{\mathcal{A}} E\alpha \left(\frac{x_2}{h} + \frac{1}{2}\right)^2 T_0 \,\mathrm{d}\mathcal{A} \\ &= bhE\alpha T_0 \int_{-1/2}^{+1/2} \left(\zeta + \frac{1}{2}\right)^2 \mathrm{d}\zeta = \frac{bh}{3} E\alpha T_0. \end{aligned}$$

and an end bending moment given by eq. (13.40),

$$\begin{aligned} Q_3^e &= -\int_{\mathcal{A}} x_2 E\alpha T \,\mathrm{d}\mathcal{A} = -\int_{\mathcal{A}} x_2 E\alpha \left(\frac{x_2}{h} + \frac{1}{2}\right)^2 T_0 \,\mathrm{d}\mathcal{A} \\ &= -bh^2 E\alpha T_0 \int_{-1/2}^{+1/2} \zeta \left(\zeta + \frac{1}{2}\right)^2 \mathrm{d}\zeta = -\frac{bh^2}{12} E\alpha T_0, \end{aligned}$$

where $\zeta = x_2/h$ is the non-dimensional coordinate through the depth of the beam.

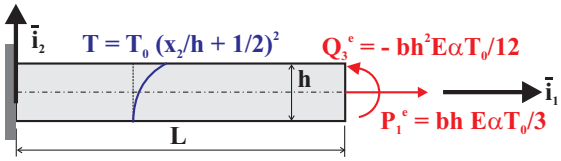

Fig. 13.21. Cantilevered beam under parabolic thermal gradient.

Because the temperature profile is independent of the axial coordinate, the equivalent thermal distributed axial and transverse loads given by eqs. (13.41) and (13.42), respectively, both vanish.

The axial displacement can be computed with the help of eq. (5.16) as $\mathrm{d}\bar{u}_1/\mathrm{d}x_1 = P_1^e/S = E\alpha T_0/3$, leading to the following displacement field

$$\bar{u}_1 = \frac{\alpha T_0 L}{3}\frac{x_1}{L}.$$

The tip axial deflection of the beam under thermal loading is $\bar{u}_{1(\mathrm{tip})} = \alpha T_0 L/3$.

Similarly, the transverse deflection of the beam is found based on eq. (5.37) as $\mathrm{d}^2\bar{u}_2/\mathrm{d}x_1^2 = Q_3^e/H_{33}^c = -\alpha T_0/h$, leading to the following transverse displacement field

$$\bar{u}_2 = -\frac{\alpha T_0 L^3}{2h}\left(\frac{x_1}{L}\right)^2.$$

The tip transverse deflection of the beam under the thermal loading is $\bar{u}_{2(\mathrm{tip})} = -\alpha T_0 L^2/(2h)$.

Finally, the stress state is found by superposition of the stresses required to inhibit thermal deformations, $\sigma_1^c = -E\alpha T$, and the stresses, σ_1^e, generated by the equivalent thermal loading, leading to

$$\sigma_1^t = -E\alpha\left(\frac{x_2}{h}+\frac{1}{2}\right)^2 T_0 + \frac{1}{3}E\alpha T_0 + E\alpha T_0\frac{x_2}{h} = \left(\frac{1}{12}-\frac{x_2^2}{h^2}\right)E\alpha T_0.$$

The first term of this expression represents the stresses that inhibit the thermal deformations, the second term is the axial stress distribution associated with the equivalent axial thermal load, P_1^e, and the last term is the axial stress distribution associated with the equivalent thermal moment, Q_3^e. The maximum axial stress is found at the top and bottom edges of the cross-section, $\sigma_{1(\mathrm{top})}^t = \sigma_{1(\mathrm{bot})}^t = -E\alpha T_0/6$, a compressive stress, whereas the axial stress in the middle of the section is $\sigma_{1(\mathrm{mid})}^t = E\alpha T_0/12$, a tensile stress.

Because only thermal loads are applied to the beam, the thermal stress field is a self-equilibrating stress field. This means that although the axial stress does not vanish, the axial force and bending moment at any cross-section do vanish; indeed, it is easy to check that

$$E\alpha T_0\int_{-h/2}^{+h/2}\left(\frac{1}{12}-\frac{x_2^2}{h^2}\right)\mathrm{d}x_2 = 0, \quad E\alpha T_0\int_{-h/2}^{+h/2} x_2\left(\frac{1}{12}-\frac{x_2^2}{h^2}\right)\mathrm{d}x_2 = 0.$$

Example 13.12. Bi-material beam under uniform temperature field

Consider the cantilevered beam of length L made of two bars, each of width b and height $h/2$, bonded together along the beam's mid-plane, as depicted in fig. 13.22. The top bar is made of a material with Young's modulus E_a and coefficient of thermal expansion α_a, and the corresponding quantities for the lower bar material are E_b and α_b, respectively. After fabrication, the temperature of the entire beam is raised by an amount T. Find the resulting axial and transverse tip deflections.

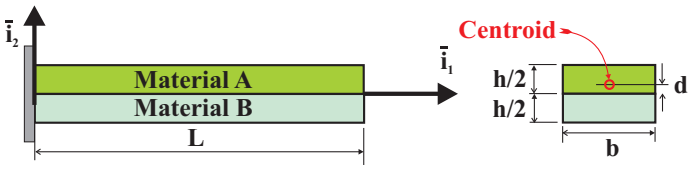

Fig. 13.22. Cantilevered bi-material beam under uniform temperature field.

The axial stiffness of the beam is $S = (E_a + E_b)bh/2$, and the centroid of the cross-section is located at a distance $d/h = (\bar{E}_a - \bar{E}_b)/4$, where $\bar{E}_a = E_a/(E_a + E_b)$ and $\bar{E}_b = E_b/(E_a + E_b)$.

The equivalent thermal loading consists of the end axial load given by eq. (13.39),

$$P_1^e = \int_{\mathcal{A}} E\alpha T \, \mathrm{d}\mathcal{A} = \int_{\mathcal{A}_a} E_a\alpha_a T \, \mathrm{d}\mathcal{A}_a + \int_{\mathcal{A}_b} E_b\alpha_b T \, \mathrm{d}\mathcal{A}_b = (E_a\alpha_a + E_b\alpha_b)\frac{bhT}{2},$$

and the end bending moment computed with respect to the geometric center of the section, given by eq. (13.40),

$$\begin{aligned} Q_3^e &= -\int_{\mathcal{A}} x_2 E\alpha T \, \mathrm{d}\mathcal{A} = -\int_{\mathcal{A}_a} x_2 E_a\alpha_a T \, \mathrm{d}\mathcal{A}_a - \int_{\mathcal{A}_b} x_2 E_b\alpha_b T \, \mathrm{d}\mathcal{A}_b \\ &= -(E_a\alpha_a - E_b\alpha_b)\frac{bh^2T}{8}. \end{aligned}$$

Because the temperature profile is independent of variable x_1, the equivalent thermal distributed axial and transverse loads given by eqs. (13.41) and (13.42), respectively, both vanish.

Under the effect of the equivalent thermal axial tip load, the axial displacement can be computed from eq. (5.16), leading to the following displacement field

$$\bar{u}_1 = (\bar{E}_a\alpha_a + \bar{E}_b\alpha_b)TL\,\eta,$$

where $\eta = x_1/L$ is the non-dimensional variable along the beam's span. The tip axial deflection of the beam's centroid under thermal loading is $\bar{u}_{1(\mathrm{tip})} = (\bar{E}_a\alpha_a + \bar{E}_b\alpha_b)TL$.

Similarly, the transverse deflection of the beam is found using eq. (5.37), leading to the following transverse displacement field

$$\bar{u}_2 = \frac{Q_3^e + dP_1^E}{2H_{33}^c} L^2 \eta^2.$$

Note that the applied equivalent thermal bending moment is computed with respect to the centroid of the section as $Q_3^e + dP_1^e$. The bending stiffness of the cross section, computed with respect to its centroid, is $H_{33}^c = bh^3(E_a^2 + E_b^2 + 14E_aE_b)/96(E_a + E_b)$. With these results, the transverse displacement field of the beam becomes

$$\bar{u}_2 = -12 \frac{E_aE_b(\alpha_a - \alpha_b)TL}{E_a^2 + E_b^2 + 14E_aE_b} \frac{L}{h} \eta^2.$$

Finally, the thermal stresses can be computed using the process described in the previous example.

13.4.4 Problems

Problem 13.10. Bi-material beam under uniform temperature field
Consider the cantilevered beam of length L made of two half-beam, each of width b and height $h/2$, welded together along the beam's mid-plane, as depicted in fig. 13.22. The top beam is made of a material with Young's modulus E_a and coefficient of thermal expansion α_a, whereas the corresponding quantities for the lower beam material are E_b and α_b, respectively. After assembly, the uniform temperature of the beam is raised by an amount T. *(1)* Find the axial force, N_1, transverse shear force, V_2, and bending moment, M_3, at the beam's mid-span. *(2)* Consider now the same bi-material beam, but fully restrained at both ends. Find the axial force, N_1, transverse shear force, V_2, and bending moment, M_3, at the beam's mid-span.

Problem 13.11. Fully restrained beam under parabolic temperature field
Consider a beam fully restrained at both ends and subject to a parabolic temperature distribution. This problem is similar to that depicted in fig. 13.21, except that the beam is now fully restrained at both ends. *(1)* Find the axial and transverse deflection of the beam under the thermal loading. *(2)* Find the thermal stress distribution in the beam. *(3)* Is this state of stress self-equilibrating?

Problem 13.12. Non-uniform fully restrained beam under parabolic temperature field
Consider the beam with a sudden change in cress-section geometry at an intermediate point and fully restrained at both ends as depicted in fig 13.23. The left portion of the beam is of length L_1 and the rectangular cross-section has a width b and height h_1, whereas the corresponding dimensions for the right portion of the beam are L_2, b and h_2, respectively. Both portions of the beam are subjected to a parabolic thermal gradient, as indicated on the figure. *(1)* Find the axial and transverse deflection fields for the beam under the thermal loading. *(2)* Plot the non-dimensional transverse displacement field, $\bar{u}_2/(L\alpha T_0)$, over the beam. *(3)* Plot the non-dimensional bending moment, $M_3/(E\alpha T_0 bL^2)$, over the beam. *(4)* Plot the non-dimensional shear force, $V_2/(E\alpha T_0 bL)$, over the beam. *(5)* Find the thermal stress distributions in the beam. *(6)* Plot the non-dimensional axial stress distribution, $\sigma_1/(E\alpha T_0)$, at $x_1 = L_1/2$ and $x_1 = L - L_2/2$. Use the following data: $\hat{h}_1 = h_1/L = 0.05$; and $\hat{h}_2 = h_2/L = 0.03$; $L = L_1 + L_2$. Consider two cases. *Case A*: $\eta_1 = L_1/L = 0.3$; $\eta_2 = L_2/L = 0.7$ and *Case B*: $\eta_1 = 0.7$; $\eta_2 = 0.3$.

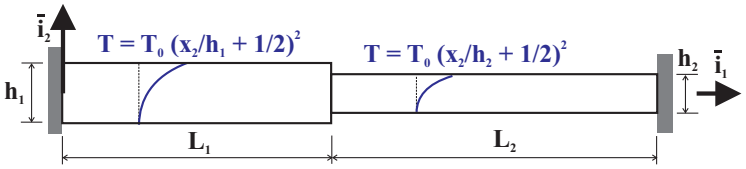

Fig. 13.23. Clamped-clamped beam subjected to parabolic thermal gradients.

Problem 13.13. Non-uniform simply supported beam under parabolic temperature field

Consider the simply supported beam with a sudden change in cress-section geometry, as depicted in fig 13.24. The left portion of the beam is of length L_1 and the rectangular cross-section has a width b and height h_1, whereas the corresponding dimensions for the right portion of the beam are L_2, b and h_2, respectively. Both portions of the beam are subjected to a parabolic thermal gradient, as indicated on the figure. *(1)* Find the axial and transverse deflection fields for the beam under the thermal loading. *(2)* Plot the non-dimensional transverse displacement field, $\bar{u}_2/(L\alpha T_0)$, over the beam. *(3)* Plot the non-dimensional bending moment, $M_3/(E\alpha T_0 bL^2)$, over the beam. *(4)* Plot the non-dimensional shear force, $V_2/(E\alpha T_0 bL)$, over the beam. *(5)* Find the thermal stress distributions in the beam. *(6)* Plot the non-dimensional axial stress distribution, $\sigma_1/(E\alpha T_0)$, at $x_1 = L_1/2$ and $x_1 = L - L_2/2$. Use the following data: $\hat{h}_1 = h_1/L = 0.05$; and $\hat{h}_2 = h_2/L = 0.03$; $L = L_1 + L_2$. Consider two cases. *Case A*: $\eta_1 = L_1/L = 0.3$; $\eta_2 = L_2/L = 0.7$ and *Case B*: $\eta_1 = 0.7$; $\eta_2 = 0.3$.

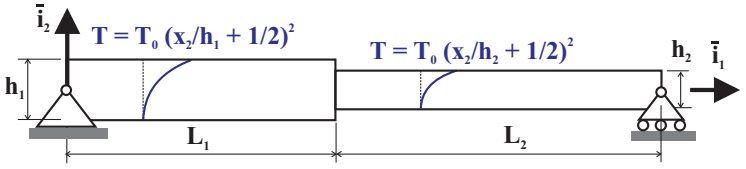

Fig. 13.24. Simply supported beam subjected to parabolic thermal gradients.

Problem 13.14. Bi-material cantilevered beam

Consider the cantilevered beam of length L made of two half-beam, each of width b and height $h/2$, welded together along the beam's mid-plane, as depicted in fig. 13.22. The top beam is made of a material of Young's modulus E_a and coefficient of thermal expansion α_a, whereas the corresponding quantities for the lower beam material are E_b and α_b, respectively. The entire assembly is heated to a uniform temperature T. *(1)* Find the transverse displacement field for the bi-material beam. *(2)* On a single graph, plot the transverse displacement field, $\bar{u}_2/(TL)$, for the six combinations of materials chosen from the materials listed in table 13.1. *(3)* What is the best combination of materials if the beam's tip deflection per degree of heating is to be maximized? *(4)* Find the thermal stress distribution in the beam. *(5)* On a single graph, plot the axial stress distribution, σ_1/T, over the cross-section the six combinations of materials chosen from the materials listed in table 13.1. *(6)* Find the location of the maximum axial stress. For what combination of materials are the thermal stresses maximized? *(7)* Check that the thermal stress field is a self-equilibrating stress field. Use $L/h = 10$.

Problem 13.15. Thermal effects in beams with unsymmetric cross-section
In example 13.10, the governing equations for beams with symmetric cross-sections are derived based on the direct method and Euler-Bernoulli kinematic assumptions. Generalize the governing equations for beam with unsymmetric cross-sections developed in chapter 6 to the case where such beams are subjected to arbitrary thermal gradients. Note that for such problems the kinematic description given in section 6.1 remains unchanged, and the equilibrium equations of the problem, see section 6.3, are still valid as well. However, the sectional constitutive laws derived in section 6.2 must be updated to accommodate thermal effects. *(1)* Derive the governing equations when principal centroidal axes of bending are used. *(2)* Derive the governing equations when centroidal axes are used that are not aligned with the principal axes of bending.

Consider now the problem of a cantilevered beam with a "Z" section as treated in example 6.6. Figure 13.25 shows the cantilevered beam subjected to the following temperature field: the top and bottom flanges are at temperatures T_t and T_b, respectively, whereas the temperature profile in the vertical web is $T = (T_t - T_b)\zeta/2 + (T_t + T_b)/2$, where $\zeta = x_3/a$. *(3)* Find the tip deflections of the beam. *(4)* Determine and plot the axial stress distribution over the cross-section of the beam. Use the following data: $T_t = \lambda T_b$, $\lambda = 3$.

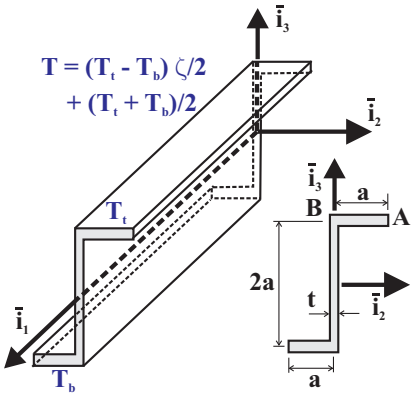

Fig. 13.25. Cantilevered beam subjected to thermal gradient.